Convex and Robust Optimization Methods for Modality Selection in External Beam Radiotherapy

Sevnaz Nourollahi

A dissertation
submitted in partial fulfillment of the
requirements for the degree of

Doctor of Philosophy

University of Washington

2018

Reading Committee:

Archis Ghate, Chair

Minsun Kim

Zelda Zabinsky

Program Authorized to Offer Degree:
Industrial & Systems Engineering

University of Washington

Abstract

Convex and Robust Optimization Methods for Modality Selection in External Beam Radiotherapy

Sevnaz Nourollahi

Chair of the Supervisory Committee:
Professor Archis Ghate
Industrial and Systems Engineering

The goal in external beam radiotherapy (EBRT) for cancer is to maximize damage to the tumor while limiting toxic effects of radiation dose on the organs-at-risk (OAR). EBRT can be delivered via different modalities such as photons, protons, and neutrons. The choice of an optimal modality depends on the anatomy of the irradiated area, and the relative physical and biological properties of the modalities under consideration. There is no single universally dominant modality.

The research objective of this dissertation is to apply convex and robust optimization methods to facilitate modality selection and corresponding dosing decisions in EBRT.
The organization of this dissertation is outlined here.

Chapter 1: Optimal modality selection The first chapter presents the first-ever mathematical formulation of the optimal modality selection problem. This formulation employs the well-known linear-quadratic (LQ) dose-response framework to model the effect of radiation on the tumor and the OAR. The chapter proves that this formulation can be tackled by solving the Karush-Kuhn-Tucker conditions of optimality, which reduce to an analytically tractable quartic equation. Extensive numerical experiments are performed to gain insights into the effect of biological and physical properties on the choice of an optimal modality or combination of modalities.

Chapter 2: Robust modality selection The feasible region and optimal solutions for the nominal modality selection problem studied in the first chapter depend on the parameters of the LQ dose-response model. Unfortunately, "true" values of these parameters are unknown. The second chapter addresses this issue by proposing a robust counterpart of the nominal formulation. As is common in the theoretical literature on robust optimization, unknown parameter values are assumed to belong to intervals. These intervals are called uncertainty sets. The chapter shows that a robust solution can be derived by solving a finite number of nominal subproblems via a KKT approach similar to the first chapter. Again, numerical experiments are performed to gain insight into the optimal choice of modality as well as the price of robustness.

Chapter 3: Spatiotemporally integrated modality selection The models in the first two chapters may be viewed as "spatiotemporally separated." In particular, base-case radiation intensity profiles that deliver base-case doses for each modality are implicitly assumed to be available to the treatment planner. Any dose different from the base-case can be administered simply by appropriately scaling the base-case intensity profiles. Consequently, the decision variables in the first two chapters correspond to the dose administered by each modality. As shown in the first two chapters, this simplification leads to analytically tractable formulations. However, recent literature on dose optimization for the *single* modality case has shown that such a simplification may result in some loss of optimality.

The third chapter therefore provides a spatiotemporally *integrated* formulation of the modality selection problem. This formulation is also based in the LQ model of dose-response. The decision variables here correspond to the fluence-maps (vectors) for each modality. The resulting model is inevitably of a larger scale and computationally more difficult than the ones in the first two chapters. Specifically, the model is a nonconvex quadratically constrained quadratic program (QCQP). An efficient method rooted in convex programming is explored for its approximate solution. Numerical experiments are performed to obtain insight into

the optimal choice of modality and its biological effect on tumor.

This dissertation establishes a mathematically rigorous foundation for modality selection and dosing in EBRT that is rooted in the clinically well-accepted LQ model of dose-response. The hope is that this foundation and associated insights via numerical experiments will help practitioners make judicious decisions while treating their patients.

TABLE OF CONTENTS

LIST OF FIGURES

LIST OF TABLES

Chapter 1

OPTIMAL MODALITY SELECTION

1.1 Introduction

External beam radiotherapy (EBRT) uses high-energy, ionizing radiation generated outside the patients, for example, by linear accelerators or cyclotrons, to kill cancerous tumor cells. Unfortunately, radiation also damages nearby organs-at-risk (OAR). Thus, the goal is to maximize the damage to the tumor while limiting below a tolerable level the toxic effects on the OAR. In an ongoing quest for attaining this goal, several modalities for delivering EBRT have been devised [7, 32, 70]. EBRT is most prevalent in the form of photon beam x-rays [33, 45]. It is also administered using beams of charged particles such as protons [30, 46, 64, 73, 76]. Heavier, carbon ions are emerging as yet another option for charged particle therapy [18, 72]. Among all patients receiving particle therapy by the end of 2013, 87.5% were treated with protons and 10.8% with carbon ions [76]. Other rarer delivery mechanisms such as neutrons, pions, boron-neutron capture therapy, and charged-nuclei therapy have also been investigated [32, 66].

Different modalities can be compared, at least in theory, based on three criteria: biological behavior, physical (dosimetric) characteristics, and cost [32, 52, 61, 66]. This dissertation focuses on the trade-offs introduced by biological and physical characteristics as described in the next two paragraphs. A cost-benefit analysis of different modalities would require entirely different techniques, and hence it is deferred to future research.

Differences in biological behavior across modalities:
Biological behavior is comprised of two main items: relative biological effectiveness (RBE), and oxygen enhancement ratio [32]. RBE captures the fact that different modalities produce

different levels of cell-damage for the same amount of physical radiation dose (measured in J/kg or Gy). Oxygen enhancement ratio is the ratio of radiation doses needed to produce the same level of tumor cell-kill in poorly oxygenated conditions as in well-oxygenated conditions. This accounts for the observation that oxygen increases radiosensitivity of tumor cells. For example, neutrons have a higher RBE and a lower oxygen enhancement ratio than photons [32, 66].

Differences in physical (dosimetric) characteristics across modalities:
The main physical characteristic of a modality is its dose depth deposition profile [32, 52, 66]. This profile describes the radiation dose deposited as a function of the distance traveled inside a medium. Photon x-rays deposit a high dose near the entry point and the dose then decreases exponentially with distance [33]. See Figure 1.1. Protons exhibit a different profile. The deposited dose abruptly reaches a peak (called the Bragg peak) deep inside the medium; and then falls sharply after the peak [18, 32, 66]. See Figure 1.2. Thus, by positioning the Bragg peak precisely in the cancerous region, a large dose differential between the tumor and the OAR can be attained. This in turn means that a large dose can be delivered to the tumor while still keeping the OAR dose within tolerable limits [30]. Carbon ions also exhibit a similar profile but with a slower post-peak drop in dose, and have a higher RBE [18, 74].

No universally superior modality:
Each modality offers certain advantages and disadvantages with respect to the above two criteria [66]. For instance, neutrons are not superior to photons or to protons in terms of their dose deposition profiles, but have a much higher RBE. This high RBE does, however, imply that neutrons are highly toxic to both the tumors and the OAR [32]. The RBE of protons is only about 10% higher than photons [57, 58, 59], but protons have a much favorable dose deposition profile as explained above. One important disadvantage with protons is that it is difficult to precisely position the Bragg peak in the cancerous region owing to various

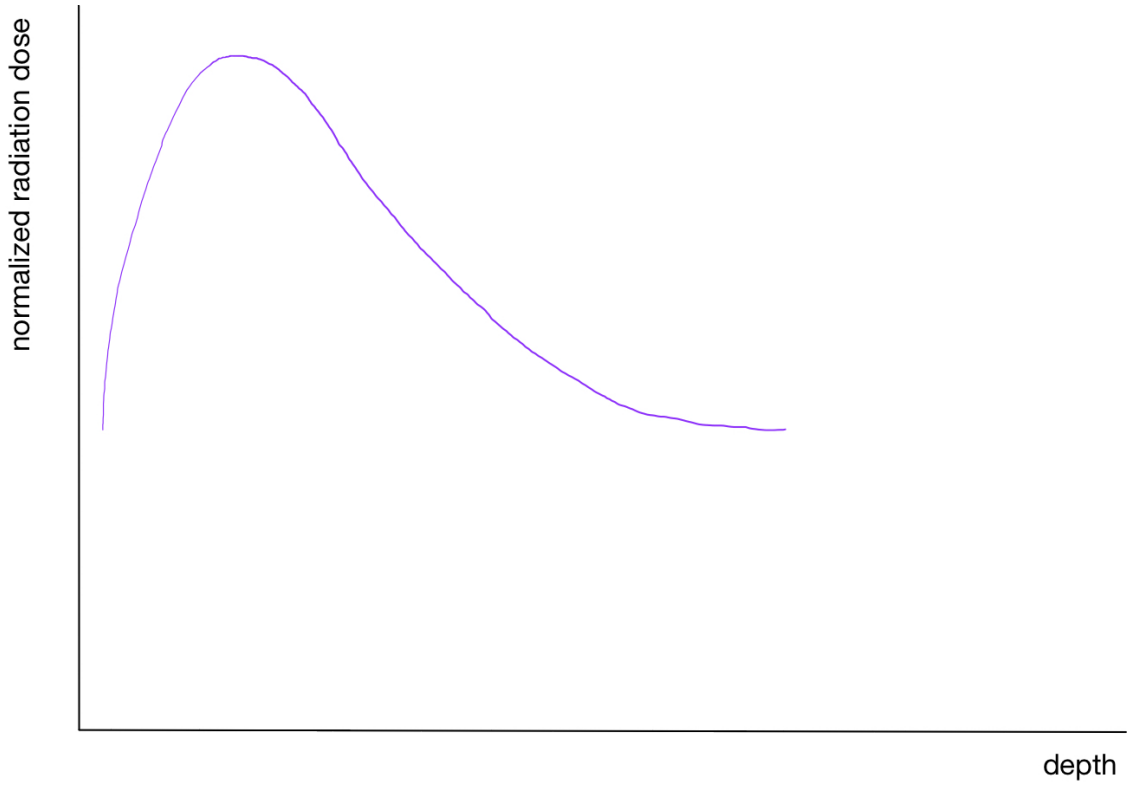

Figure 1.1: A schematic of photon dose depth deposition profile.

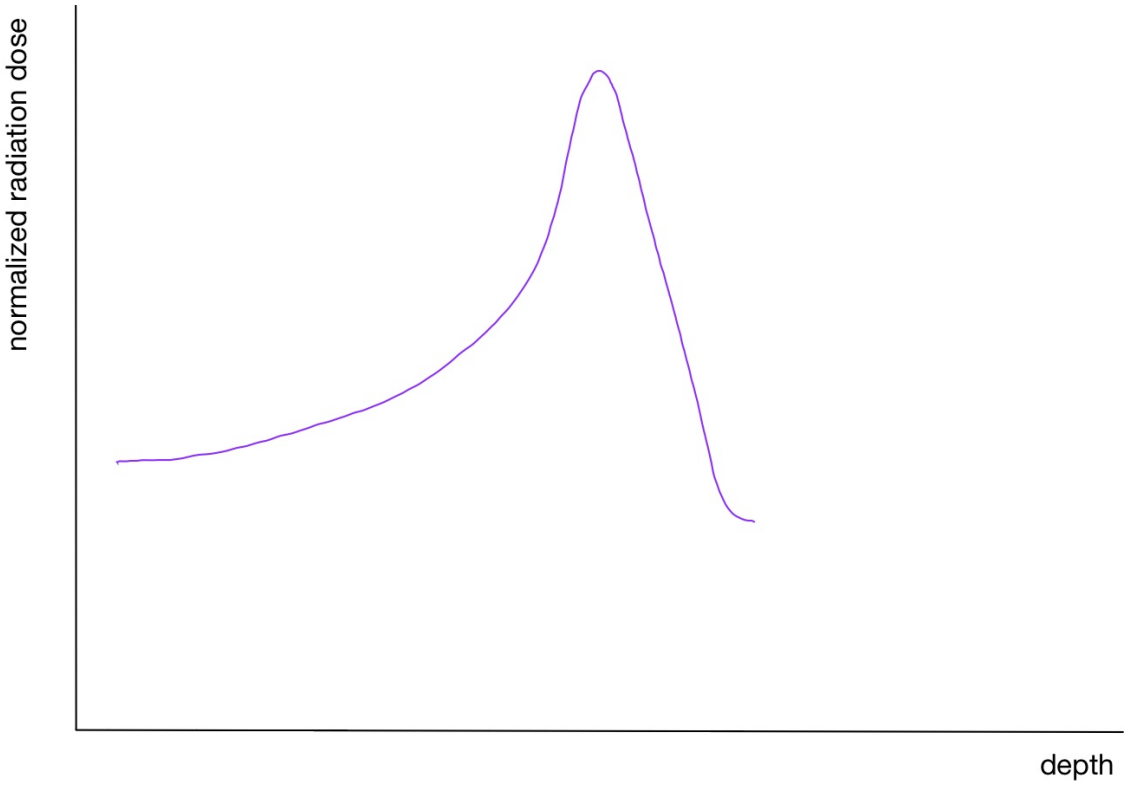

Figure 1.2: A schematic of proton dose depth deposition profile.

uncertainties; thus the risk of a high OAR toxicity has to be carefully managed [7, 56]. Treatment with protons and other charged particles is also currently much more expensive than photon therapy [46, 63]. In addition, due to the longest history of using photons in cancer treatments, the most sophisticated ancillary systems are currently available for photon EBRT to aid precise localization of the tumors, e.g., image-guided radiotherapy.

No clear winner that dominates all other modalities in all three criteria has emerged thus far. This was summarized by Halperin [32] a decade ago: "*Neutrons, photons, pions, alpha particles, stripped nuclei, protons, and electrons vary in their biological, physical, and cost characteristics. None has yet met the test of being the generic ideal particle. Instead, each of these particles will probably offer advantages for particular histological types of cancer, at specific stages, in certain clinical conditions. An understanding of the biology of tumours should help to clarify the ideal particle for a clinical situation. Much of the history of the search for the ideal particle has yet to be created.*" A similar sentiment was reiterated by McDermott [51] and by Schulz and Kagan [72] in 2016, and by Baumann et al. [7] in 2017. Missing a universally superior EBRT modality, some studies have considered combinations of two modalities (typically photons and protons) to leverage their physical and biological advantages [10, 13, 15, 16, 17, 19, 48, 77, 86].

Lack of randomized clinical trials:

One hurdle in deciding an ideal modality or a combination of two modalities is that no randomized clinical trial results comparing outcomes of different modalities are currently available. For instance, the prevalent EBRT modality for prostate cancer is still photons, but it is also where proton therapy has been used most widely (Mitin and Zietman [52] reported that 70% of patients who received proton therapy by 2014 had prostate cancer). Nevertheless, in January 2016, Schiller et al. [71] stated: "*There are still no completed randomized trials comparing proton-beam therapy with photon-beam therapy in men with clinically localized prostate cancer.* A year later, this has not changed. Indeed, in February 2017, Tyson et al. [79] commented: "*Although there is some evidence that novel radiation*

therapies may improve the dose distribution with higher doses delivered locally to the tumor thereby preserving surrounding healthy tissues, these assertions remain unproven in studies to date ... . there are no randomized clinical trials comparing proton therapy to conventional radiation therapy." This lack of randomized clinical trials extends to other cancers where the use of proton beams is rarer than prostate. For example, after a retrospective comparison between photons and protons for 243,822 non-small cell lung cancer patients in the National Cancer Database (photons: 243,474; protons: 348), Higgins et al. [34] stated in January 2017 that "*further validation in the randomized setting is needed.*" Similarly, Ramaekers et al. [64] performed a meta-analysis of 86 observational studies (74 photon, 5 carbon ion and 7 proton) on head-and-neck cancers and concluded in 2010: "*several reviews indicated that based on clinical evidence it remains unclear, mainly because of the absence of randomized trials, whether particle therapy is superior over radiotherapy with photons ...* ." A similar observation was repeated four years later by Ahn et al. [2]. This situation might not significantly change in the near future, given the ethical, financial, and logistical difficulties involved in the design of randomized clinical trials [14, 28, 44, 54, 82].

Further challenges posed by fractionation:

The selection of an appropriate modality is further complicated because radiotherapy is typically administered in multiple treatment sessions over several weeks. This is called fractionation. Healthy tissues possess better damage-repair capabilities than tumors [31, 84]. Fractionation thus gives healthy tissue time to recover between treatment sessions. For any single radiation modality, the optimal number of fractions and the corresponding dose in each fraction depend on (i) the relative difference between the tumor's and the healthy tissue's biological response to that modality, (ii) the dose deposition profile of that modality with respect to the anatomy of the irradiated area, and (iii) the tumor proliferation rate. The tradeoffs in determining an optimal number of fractions and doses have been studied over the last several decades mainly for photon therapy [1, 4, 5, 6, 9, 11, 20, 21, 22, 23, 25, 26, 27, 35, 36, 37, 38, 39, 40, 50, 53, 65, 67, 68, 69, 78, 80, 81, 85].

Literature on mathematical optimization models for single-modality fractionation:

Given the aforementioned difficulties in designing randomized clinical trials, many of the above studies formulate and solve theoretical optimization models of the single modality fractionation problem to guide decisions. These formulations are based on the well-known linear-quadratic (LQ) model of radiation dose response [31]. The RBE of radiation on both the tumor and the OAR is captured via the α and β parameters of the LQ response model. The dose deposition profile is modeled via the so-called sparing factors, which equal the ratio of doses delivered to the tumor and to various OAR. The goal is to minimize the fraction of surviving tumor cells subject to upper limit constraints on the biological effect (BE) [31] delivered to various OAR. This results in a non-convex quadratically constrained quadratic programming problem (QCQP). Such problems in general belong to the class NP-hard [47]. Existing work on solving this theoretical single modality fractionation model thus includes various heuristic and exact solution methods that exploit the structure of its formulation. For example, a closed-form solution is derived in [11, 23, 25, 38, 53, 68, 80] for the case of a single OAR; a simulated annealing heuristic is used in [85] and Karush-Kuhn-Tucker (KKT) conditions are employed in [9] for an extension with two OAR; we have shown in [68] that an exact solution can be derived for the case of multiple OAR using KKT conditions when problem parameters are ordered a certain way; it is shown in [6, 67] that the problem with multiple OAR can be solved to optimality by reformulating it as a two-variable linear program. When two modalities are available, additional tradeoffs arising from their RBE and dose deposition profiles need to be considered. To the best of our knowledge, no existing mathematical work has modeled this fractionation problem with two modalities.

Contributions of this chapter:

In Section 1.2 of this chapter, we provide a mathematical formulation of the fractionation problem with two modalities, where the goal is to find an optimal number of treatment

sessions and the corresponding dose per session for each modality. We show that KKT conditions for this formulation can be tackled by solving an analytically tractable quartic equation. In Section 1.3, we perform sensitivity analyses to gain insight into the effect of problem parameters on the choice of optimal modalities. These parameters characterize biological and physical behaviors of the two modalities under consideration. In one set of sensitivity analyses (Section 1.3.1), we consider two modalities that have comparable physical characteristics but distinct biological characteristics. One example of this could be photons and neutrons. In the second set of sensitivity analyses (Section 1.3.2), we consider two modalities that have comparable biological characteristics but distinct physical characteristics. One example of this could be photons and protons. This "one-at-a-time" manner of performing sensitivity analyses facilitates the interpretation of results, although it is not a requirement of our mathematical model itself. Finally, although our initial formulation focuses on the single OAR case for ease of exposition, we briefly describe how our KKT approach can be extended to multiple OAR in Section 1.4. We conclude in that section by outlining opportunities for future work.

1.2 Problem formulation and solution method

In this section, we provide a formulation of the fractionation problem with two modalities using the LQ dose-response model. We use notation that is standard in the single modality fractionation literature, except that, in our case, modalities are indexed by $i = 1, 2$. Modality 1 is assumed to be the "conventional" modality such as photon EBRT. Let N_i denote the number of treatment sessions administered (once daily) with modality i. Similarly, let d_i denote the tumor-dose in each one of the N_i sessions for modality i. Moreover, $\alpha_i^\tau, \beta_i^\tau$ denote the parameters of the tumor's LQ dose-response model for modality i. Notation $\pi(N_1 + N_2)$ represents tumor proliferation over a treatment course that includes $N_1 + N_2$ sessions. We employ a particular form for the proliferation function $\pi(\cdot)$ in our numerical results later; in this section, we simply emphasize that it depends on the length of the treatment course as is standard in the literature. Let s_i denote the OAR's sparing factor for modality i. That

is, the dose to OAR i equals $s_i d_i$. A procedure for calculating sparing factors is described in [68]. Let $\alpha_i^\phi, \beta_i^\phi$ denote the OAR's LQ dose-response parameters for modality i. Suppose that the OAR is known to tolerate a dose of d_{conv} per session when administered using the conventional modality 1 in N_{conv} sessions. Then, the BE of this conventional treatment plan equals $B = N_{\text{conv}}\alpha_1^\phi d_{\text{conv}} + N_{\text{conv}}\beta_1^\phi (d_{\text{conv}})^2$. As in [69], let $N_{\max}$ denote the maximum total number of treatment sessions that is feasible to administer (based on logistical or other clinical factors). The thought process in our stylized formulation is that s_1, s_2 characterize the physical properties of the two modalities, whereas α, β, and τ correspond to the biological ones.

We pursue the standard approach of minimizing the fraction of surviving tumor cells subject to the constraint that the BE of the treatment plan is no more than the conventional BE that the OAR is known to tolerate. This yields the formulation

$$(P) \quad \min_{N_1, d_1, N_2, d_2} e^{-N_1\alpha_1^\tau d_1 - N_1\beta_1^\tau (d_1)^2 - N_2\alpha_2^\tau d_2 - N_2\beta_2^\tau (d_2)^2 + \pi(N_1+N_2)} \tag{1.1}$$

$$N_1 s_1 \alpha_1^\phi d_1 + N_1\beta_1^\phi (s_1 d_1)^2 + N_2\alpha_2^\phi d_2 + N_2\beta_2^\phi (s_2 d_2)^2 \leq B, \tag{1.2}$$

$$d_1 \geq 0, \tag{1.3}$$

$$d_2 \geq 0, \tag{1.4}$$

$$N_1 + N_2 \leq N_{\max}, \tag{1.5}$$

$$0 \leq N_1 \text{ integer}, \tag{1.6}$$

$$0 \leq N_2 \text{ integer}. \tag{1.7}$$

We make a few observations about this problem. It can be tackled by first solving the indexed group of problems

$$(P(N_1, N_2)) \quad \min_{d_1, d_2} e^{-N_1\alpha_1^\tau d_1 - N_1\beta_1^\tau (d_1)^2 - N_2\alpha_2^\tau d_2 - N_2\beta_2^\tau (d_2)^2 + \pi(N_1+N_2)} \tag{1.8}$$

$$N_1 s_1 \alpha_1^\phi d_1 + N_1\beta_1^\phi (s_1 d_1)^2 + N_2\alpha_2^\phi d_2 + N_2\beta_2^\phi (s_2 d_2)^2 \leq B, \tag{1.9}$$

$$d_1 \geq 0, \tag{1.10}$$

$$d_2 \geq 0, \tag{1.11}$$

for all nonnegative integer pairs (N_1, N_2) such that $0 \leq N_1 + N_2 \leq N_{\max}$. In particular, let $d_1^*(N_1, N_2)$ and $d_2^*(N_1, N_2)$ denote optimal doses for modalities $1, 2$ in problem $(P(N_1, N_2))$, respectively. Let $F^*(N_1, N_2)$ denote the optimal objective value of problem $(P(N_1, N_2))$. Then, problem (P) can be solved by minimizing $F^*(N_1, N_2)$ over all integer pairs (N_1, N_2) such that $0 \leq N_1 + N_2 \leq N_{\max}$. If the pair N_1^*, N_2^* is optimal for this problem, then the quadruple $N_1^*, d_1^*(N_1^*, N_2^*), N_2^*, d_2^*(N_1^*, N_2^*)$ is optimal for problem (P). Since the exponential function is monotonic in its argument, minimizing the objective function in $(P(N_1, N_2))$ is equivalent to minimizing $-N_1\alpha_1^\tau d_1 - N_1\beta_1^\tau (d_1)^2 - N_2\alpha_2^\tau d_2 - N_2\beta_2^\tau (d_2)^2 + \pi(N_1 + N_2)$. Further, since the pair N_1, N_2 is fixed in problem $(P(N_1, N_2))$, the proliferation term $\pi(N_1 + N_2)$ is a constant that can be ignored without loss of optimality. Finally, the objective function is decreasing in d_1 and d_2 and the left hand side of constraint (1.9) is increasing in d_1 and d_2. Thus, constraint (1.9) must be active at an optimal solution. In other words, solving $(P(N_1, N_2))$ is equivalent to solving

$$(Q(N_1, N_2)) \quad \min_{d_1, d_2} - \left(N_1\alpha_1^\tau d_1 + N_1\beta_1^\tau (d_1)^2 + N_2\alpha_2^\tau d_2 + N_2\beta_2^\tau (d_2)^2\right) \tag{1.12}$$

$$N_1 s_1 \alpha_1^\phi d_1 + N_1\beta_1^\phi (s_1 d_1)^2 + N_2\alpha_2^\phi d_2 + N_2\beta_2^\phi (s_2 d_2)^2 = B, \tag{1.13}$$

$$d_1 \geq 0, \tag{1.14}$$

$$d_2 \geq 0. \tag{1.15}$$

The rest of this section develops a solution method based on KKT conditions for $(Q(N_1, N_2))$.

There are three possibilities: $d_1 > 0, d_2 = 0$; $d_1 = 0, d_2 > 0$; and $d_1 > 0, d_2 > 0$. In the first two cases, the problem reduces to a single modality problem, which can be solved simply by solving a quadratic equation derived from constraint (1.13). Specifically, in the first case, a candidate d_1 is given by

$$d_1 = \frac{-N_1 s_1 \alpha_1^\phi + \sqrt{N_1^2 s_1^2 (\alpha_1^\phi)^2 + 4N_1\beta_1^\phi s_1^2 B}}{2N_1\beta_1^\phi (s_1)^2}. \tag{1.16}$$

In the second case, a candidate d_2 is given by

$$d_2 = \frac{-N_2 s_2 \alpha_2^\phi + \sqrt{N_2^2 s_2^2 (\alpha_2^\phi)^2 + 4N_2\beta_2^\phi s_2^2 B}}{2N_2\beta_2^\phi (s_2)^2}. \tag{1.17}$$

In order to explore the third case, we attach Lagrange multipliers λ, μ_1, and μ_2 with the three constraints (1.9)-(1.11), respectively. Then, KKT conditions (see Equations (5.49) on page 243 of Boyd [12]) for this problem can be written as: $\mu_1 \geq 0$, $\mu_2 \geq 0$, $\mu_1 d_1 = 0$, $\mu_2 d_2 = 0$, $d_1 \geq 0$, $d_2 \geq 0$, and

$$N_1 s_1 \alpha_1^\phi d_1 + N_1 \beta_1^\phi (s_1 d_1)^2 + N_2 s_2 \alpha_2^\phi d_2 + N_2 \beta_2^\phi (s_2 d_2)^2 = B, \tag{1.18}$$

$$\begin{bmatrix} -\mu_1 \\ -\mu_2 \end{bmatrix} + \lambda \begin{bmatrix} N_1 s_1 \alpha_1^\phi + 2N_1 \beta_1^\phi s_1^2 d_1 \\ N_2 s_2 \alpha_2^\phi + 2N_2 \beta_2^\phi s_2^2 d_2 \end{bmatrix} = \begin{bmatrix} N_1 \alpha_1^\tau + 2N_1 \beta_1^\tau d_1 \\ N_2 \alpha_2^\tau + 2N_2 \beta_2^\tau d_2 \end{bmatrix}. \tag{1.19}$$

Since $d_1 > 0$ and $d_2 > 0$, we know that $\mu_1 = \mu_2 = 0$. Substituting this into the system (1.19) of equations yields

$$d_1 = \frac{\lambda s_1 \alpha_1^\phi - \alpha_1^\tau}{2(\beta_1^\tau - \lambda \beta_1^\phi s_1^2)}, \tag{1.20}$$

$$d_2 = \frac{\lambda s_2 \alpha_2^\phi - \alpha_2^\tau}{2(\beta_2^\tau - \lambda \beta_2^\phi s_2^2)}. \tag{1.21}$$

Substituting this back into (1.18) yields the following quartic equation

$$\lambda^4\Big(-16B(\beta_1^\phi)^2(\beta_2^\phi)^2s_1^4s_2^4-4(\alpha_1^\phi)^2\beta_1^\phi(\beta_2^\phi)^2N_1s_1^4s_2^4-4(\alpha_2^\phi)^2\beta_2^\phi(\beta_1^\phi)^2N_2s_2^4s_1^4\Big)+$$
$$\lambda^3\Big(32B(\beta_1^\phi)^2\beta_2^\phi\beta_2^\tau s_1^4s_2^2+16(\alpha_1^\phi)^2\beta_1^\phi(\beta_2^\phi)^2N_1s_1^4s_2^2-8(\alpha_1^\phi)^2\beta_1^\phi\beta_2^\phi\beta_2^\tau N_1s_1^4s_2^2$$
$$+8(\alpha_2^\phi)^2(\beta_1^\phi)^2\beta_2^\tau N_2s_1^4s_2^2+32B\beta_1^\phi\beta_1^\tau(\beta_2^\phi)^2s_1^2s_2^4+8(\alpha_1^\phi)^2\beta_1^\tau(\beta_2^\phi)^2N_1s_1^2s_2^4$$
$$16(\alpha_2^\phi)^2(\beta_1^\phi)^2\beta_2^\phi N_2s_1^2s_2^4-8(\alpha_2^\phi)^2\beta_1^\phi\beta_1^\tau\beta_2^\phi N_2s_1^2s_2^4\Big)+$$
$$\lambda^2\Big(-16B(\beta_1^\phi)^2(\beta_2^\tau)^2s_1^4-8(\alpha_1^\phi)^2\beta_1^\phi(\beta_2^\phi)^2N_1s_1^4+4(\alpha_1^\phi)^2\beta_1^\phi(\beta_2^\tau)^2N_1s_1^4$$
$$-8\alpha_2^\phi\alpha_2^\tau(\beta_1^\phi)^2\beta_2^\tau N_2s_1^4s_2-64B\beta_1^\phi\beta_1^\tau\beta_2^\phi\beta_2^\tau s_1^2s_2^2-16(\alpha_1^\phi)^2\beta_1^\tau(\beta_2^\phi)^2N_1s_1^2s_2^2$$
$$-16(\alpha_2^\phi)^2(\beta_1^\phi)^2\beta_2^\tau N_2s_1^2s_2^2-16\alpha_1^\phi\alpha_1^\tau\beta_1^\phi(\beta_2^\phi)^2N_1s_1^3s_2^2+16\alpha_1^\phi\alpha_1^\tau\beta_1^\phi\beta_2^\phi\beta_2^\tau N_1s_1^3s_2^2$$
$$+4(\alpha_2^\tau)^2(\beta_1^\phi)^2\beta_2^\phi N_2s_1^4s_2^2-16\alpha_2^\phi\alpha_2^\tau(\beta_1^\phi)^2\beta_2^\phi N_2s_1^2s_2^3+16\alpha_2^\phi\alpha_2^\tau\beta_1^\phi\beta_1^\tau\beta_2^\phi N_2s_1^2s_2^3$$
$$-16B(\beta_1^\tau)^2(\beta_2^\phi)^2s_2^4-8(\alpha_2^\phi)^2(\beta_1^\phi)^2\beta_2^\phi N_2s_2^4+4(\alpha_2^\phi)^2(\beta_1^\tau)^2\beta_2^\phi N_2s_2^4$$
$$-8\alpha_1^\phi\alpha_1^\tau\beta_1^\tau(\beta_2^\phi)^2N_1s_1s_2^4+4(\alpha_1^\tau)^2\beta_1^\phi(\beta_2^\phi)^2N_1s_1^2s_2^4\Big)+$$
$$\lambda\Big(32B\beta_1^\phi\beta_1^\tau(\beta_2^\tau)^2s_1^2+8(\alpha_1^\phi)^2\beta_1^\tau(\beta_2^\phi)^2N_1s_1^2+8\alpha_1^\phi\alpha_1^\tau\beta_1^\phi(\beta_2^\phi)^2N_1s_1^3$$
$$-8\alpha_1^\phi\alpha_1^\tau\beta_1^\phi(\beta_2^\tau)^2N_1s_1^3+16\alpha_2^\phi\alpha_2^\tau(\beta_1^\phi)^2\beta_2^\tau N_2s_1^2S_2+32B(\beta_1^\tau)^2\beta_2^\phi\beta_2^\tau s_2^2+$$
$$8(\alpha_2^\phi)^2(\beta_1^\phi)^2\beta_2^\tau N_2s_2^2+16\alpha_1^\phi\alpha_1^\tau\beta_1^\tau(\beta_2^\phi)^2N_1s_1s_2^2-8(\alpha_1^\tau)^2\beta_1^\phi\beta_2^\phi\beta_2^\tau N_1s_1^2s_2^2$$
$$-8(\alpha_2^\tau)^2\beta_1^\phi\beta_1^\tau\beta_2^\phi N_2s_1^2s_2^2+8\alpha_2^\phi\alpha_2^\tau(\beta_1^\phi)^2\beta_2^\phi N_2s_2^3-8\alpha_2^\phi\alpha_2^\tau(\beta_1^\tau)^2\beta_2^\phi N_2s_2^3\Big)+$$
$$\Big(-16B(\beta_1^\tau)^2(\beta_2^\tau)^2-8\alpha_1^\phi\alpha_1^\tau\beta_1^\tau(\beta_2^\phi)^2N_1s_1+4(\alpha_1^\tau)^2\beta_1^\phi(\beta_2^\tau)^2N_1s_1^2$$
$$-8\alpha_2^\phi\alpha_2^\tau(\beta_1^\phi)^2\beta_2^\tau N_2s_2+4(\alpha_2^\tau)^2(\beta_1^\tau)^2\beta_2^\phi N_2s_2^2\Big)=0.$$

This quartic equation can be easily solved analytically or numerically. Its real roots can then be substituted back into (1.20)-(1.21) to obtain candidate solutions. After solving the quartic equation, there are four possible cases for each real root that need to be considered separately based on the form of Equations (1.20)-(1.21).

1. $\lambda=\beta_1^\tau/(\beta_1^\phi s_1^2)=\alpha_1^\tau/(s_1\alpha_1^\phi)$.

   (a) $\lambda=\beta_2^\tau/(\beta_2^\phi s_2^2)$.

i. $\lambda = \alpha_2^\tau/(\alpha_2^\phi s_2)$.

The only way this can happen is if the two modalities behave identically, in the sense that $\frac{\alpha_1^\tau}{(\alpha_1^\phi s_1)} = \frac{\alpha_2^\tau}{(\alpha_2^\phi s_2)} = \frac{\beta_1^\tau}{(\beta_1^\phi s_1^2)} = \frac{\beta_2^\tau}{(\beta_2^\phi s_2^2)} = c$, for some constant c. In fact, in this case, we do not even need the KKT conditions, since problem $(P(N_1, N_2))$ can be rewritten by replacing α_1^τ and β_1^τ with $\alpha_1^\phi s_1 c$ and $\beta_1^\phi s_1^2 c$, respectively. This yields

$$\begin{aligned} &\min \ -cB \\ N_1 s_1 \alpha_1^\phi d_1 + N_1 \beta_1^\phi (s_1 d_1)^2 + N_2 s_2 \alpha_2^\phi d_2 + N_2 \beta_2^\phi (s_2 d_2)^2 &= B, \\ &d_1, d_2 \geq 0. \end{aligned}$$

Thus, all feasible solutions are optimal as they all have the same objective function value of $-cB$ (note that the problem does have feasible solutions, for example, $d_2 = 0$ and d_1 obtained by solving a quadratic equation).

ii. $\lambda \neq \alpha_2^\tau/(\alpha_2^\phi s_2)$.

This situation does not yield a feasible d_2, because the denominator in Equation (1.21) is zero but the numerator is not. Thus this case does not yield any candidate solutions.

(b) $\lambda \neq \beta_2^\tau/(\beta_2^\phi s_2^2)$.

i. $\lambda = \alpha_2^\tau/(\alpha_2^\phi s_2)$.

This implies from Equation (1.21) that $d_2 = 0$. This is contrary to the assumed scenario that $d_1 > 0$ and $d_2 > 0$. Thus this case does not yield any candidate solutions.

ii. $\lambda \neq \alpha_2^\tau/(\alpha_2^\phi s_2)$.

In this case, we can obtain d_2 from Equation (1.21), substitute its value into Equation (1.18), and solve a quadratic equation to get d_1. That is,

$$d_1 = \frac{-N_1 s_1 \alpha_2^\phi + \sqrt{N_1^2 s_1^2 (\alpha_1^\phi)^2 + 4 N_1 \beta_1^\phi s_1^2 (B - N_2 s_2 \alpha_2^\phi d_2 - N_2 \beta_2^\phi s_2^2 d_2^2)}}{2 N_1 \beta_1^\phi s_1^2}. \tag{1.22}$$

2. $\lambda = \beta_1^\tau/(\beta_1^\phi s_1^2)$ and $\lambda \neq \alpha_1^\tau/(\alpha_1^\phi s_1)$.

   This situation does not yield a feasible d_1 because the denominator in Equation (1.20) is zero but the numerator is not. Thus this case does not yield any candidate solutions.

3. $\lambda \neq \beta_1/(\beta_1^\phi s_1^2)$ and $\lambda = \alpha_1^\tau/(\alpha_1^\phi s_1)$.

   This implies from Equation (1.20) that $d_1 = 0$. This is contrary to the assumed scenario that $d_1 > 0$ and $d_2 > 0$. Thus this case does not yield any candidate solutions.

4. $\lambda \neq \beta_1^\tau/(\beta_1^\phi s_1^2)$ and $\lambda \neq \alpha_1^\tau/(\alpha_1^\phi s_1)$.

   (a) $\lambda = \beta_2^\tau/(\beta_2^\phi s_2^2)$.

      i. $\lambda = \alpha_2^\tau/(\alpha_2^\phi s_2)$.

         Here, d_1 can be obtained from (1.20). We can substitute its value into Equation (1.18), and solve a quadratic equation to calculate d_2. That is,

$$d_2 = \frac{-N_2 s_2 \alpha_1^\phi + \sqrt{N_2^2 s_2^2 (\alpha_2^\phi)^2 + 4N_2 \beta_2^\phi (s_2)^2 (B - N_1 s_1 \alpha_1^\phi d_1 - N_1 \beta_1^\phi s_1^2 d_1^2)}}{2N_2 \beta_2^\phi (s_2)^2}. \tag{1.23}$$

      ii. $\lambda \neq \alpha_2^\tau/(\alpha_2^\phi s_2)$.

         Here, we cannot obtain any feasible d_2 because the denominator in Equation (1.21) is zero but the numerator is not. Thus, this case does not yield any candidate solutions.

   (b) $\lambda \neq \beta_2^\tau/(\beta_2^\phi s_2^2)$.

      i. $\lambda = \alpha_2^\tau/(\alpha_2^\phi s_2)$.

         Here, Equation (1.21) yields $d_2 = 0$. This is contrary to the assumed scenario that $d_1 > 0$ and $d_2 > 0$. Thus this case does not yield any candidate solutions.

      ii. $\lambda \neq \alpha_2^\tau/(\alpha_2^\phi s_2)$.

         In this case, d_1 and d_2 can be obtained from Equations (1.20)-(1.21).

The objective values of all candidate solutions can then be compared to find an optimal solution. This solution method is applied to perform numerical sensitivity analyses in the next section.

1.3 Numerical results

Let M_1 denote a conventional modality such as photon EBRT, and let M_2 denote an alternative modality. Table 1.1 illustrates a legend for three colors that will be employed throughout this section to indicate the use of modalities M_1, (M_1, M_2) mixture, and M_2, respectively.

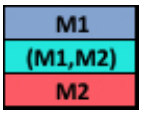

Table 1.1: Legend of colors showing three different modality choices.

Our numerical results are categorized into two parts that are presented in Sections 1.3.1 and 1.3.2, respectively. Section 1.3.1 investigates the trade-offs between M_1 and a biologically superior M_2. Section 1.3.2 studies the trade-offs between M_1 and a physically superior M_2. Recall that biological and physical are the two main characteristics of a modality as described in Section 1.1. As stated in Section 1.1, we pursue this one-at-a-time method of performing sensitivity analyses because it facilitates interpretation of our results. In both Sections 1.3.1 and 1.3.2, these trade-offs are explored for different values of a biological parameter $r = \alpha_2^{\phi}/\alpha_2^{\tau}$ that we introduce in this chapter. The thought process behind this parameter is as follows. A biologically superior modality will inflict a higher damage on both the tumor and the OAR. The ratio r attempts to capture the differential in the damage to the tumor and the OAR. As r increases, the damage to the OAR relative to the damage to the tumor using M_2 increases, when all other things are equal. Thus, M_2 becomes less desirable as r increases. For the conventional modality M_1, we used $s_1 = 1$ as the base-value of physical

$\alpha_1^\tau = 0.35$ Gy^{-1}	$\beta_1^\tau = 0.035$ Gy^{-2}
$\alpha_1^\phi = 0.35$ Gy^{-1}	$\beta_1^\phi = 0.175$ Gy^{-2}

Table 1.2: Parameters for the conventional modality M_1.

characteristics throughout this chapter. Also, for M_1, we used $\alpha_1^\tau/\beta_1^\tau = 10$ Gy, $\alpha_1^\phi/\beta_1^\phi = 2$ Gy, and the OAR tolerance was assumed to be $N_{\text{conv}}d_{\text{conv}} = 50$ Gy delivered in $N_{\text{conv}} = 25$ fractions [31, 49]. Table 1.2 shows other specific parameter values for M_1. These values are standard in the clinical literature [22, 23, 31, 49], and yield $B = 35$ as the right hand side of constraint (1.2). Similarly, β_2^ϕ was fixed at 0.175 Gy^{-2} and β_2^τ was fixed at 0.035 Gy^{-2} throughout this chapter.

For the tumor repopulation term $\pi(N_1 + N_2)$ in the expression for BE in the objective function of problem (P), we used

$$\pi(N_1 + N_2) = \frac{[(N_1 + N_2) - 1 - T_{\text{lag}}]^+ \ln 2}{T_d}, \tag{1.24}$$

where T_d and T_{lag} are tumor doubling time and lag time, respectively; and $[\cdot]^+ = \max(\cdot, 0)$. This functional form for tumor repopulation is common in the literature [22, 31], and it assumes that tumor repopulation does not start until T_{lag} days after treatment begins.

In this study, we present results with $T_d = 3$ days and $T_{\text{lag}} = 0$ day as representative values since qualitative trends in our results were invariant with respect to these numbers. We fixed $N_{\max}$ at 200 days throughout.

Our evaluation criterion equals the ratio of surviving cells attained by an optimal modality relative to that attained by the conventional modality. We assume that "standard practice" delivers radiotherapy using conventional modality (M_1) only for 25 fractions, i.e., $N_{\text{conv}} = 25$. We compute the ratio of surviving cells in three ways. First, we fix the number of treatment sessions to $N_{\text{conv}} = 25$, and compute the ratio of surviving cells attained by an optimal modality relative to that attained by the conventional modality. This amounts to comparing

the effect of optimizing the choice of modality (without optimizing the number of sessions) against standard practice. Second, we re-compute this ratio, but this time by also optimizing the number of sessions in the numerator. This amounts to comparing the effect of solving problem (P) against standard practice. Finally, we calculate this ratio again, but this time by also optimizing the number of sessions in the denominator.

1.3.1 Biologically superior modality M_2 combined with conventional modality M_1

In this section, we investigate the case where M_2 is biologically superior to M_1 (when $r = 1$) as characterized by higher values of α_2^τ in the range $0.35-0.8$ Gy^{-1}. The physical characteristics of M_2 are assumed to be similar to M_1 and hence s_2 is fixed at 1 in this section. For example, this section therefore studies trade-offs between conventional photon EBRT and neutrons. Results are summarized in Tables 1.3-1.6.

Table 1.3 shows the ratio of surviving cells when an optimal modality (or combination) is used with the total number of fractions fixed at $N_{\text{conv}} = 25$, relative to the standard practice of using M_1 with $N_{\text{conv}} = 25$ fractions. The table shows that for a fixed α_2^τ, the optimal modality switches from M_2 to M_1 as r increases since the relative damage to the OAR from M_2 becomes larger, making M_2 less desirable. For a fixed r, the optimal modality switches from M_1 to M_2 as α_2^τ increases since the biological power of M_2 becomes larger. Therefore, for sufficiently low fixed values of r, i.e., when the damage to the OAR from M_2 is relatively lower than the damage to the tumor, M_2 dominates M_1 for all values of α_2^τ because of M_2's superior biological power ($\alpha_2^\tau > \alpha_1^\tau$). Similarly, M_1 dominates M_2 for all values of α_2^τ for sufficiently high values of r due to the high toxicity to the OAR from M_2. The switch from M_1 to M_2 occurs at higher values of α_2^τ as r increases. This is because, the biological power of M_2, that is, α_2^τ has to be sufficiently high for that modality to become desirable despite its higher damage to the OAR (large r). Similarly, the switch from M_2 to M_1 occurs at higher values of r as α_2^τ increases. For each fixed value of α_2^τ, the surviving cell ratio is nondecreasing as r increases because M_2 becomes less desirable. Similarly, for each fixed value of r, the surviving cell ratio is nonincreasing as α_2^τ increases because M_2 becomes more

desirable.

Table 1.4 shows optimal modalities and the optimal number of fractions obtained by solving problem (P) (in contrast with Table 1.3 wherein the number of fractions is not optimized). The qualitative trends in the choice of optimal modality are identical to that in Table 1.3 as expected. Moreover, for each fixed α_2^τ, the optimal number of fractions is nonincreasing as r increases when M_2 is the optimal modality. This may be because as M_2 damages the OAR more and more relative to the tumor, prolonged fractionation is less desirable. For each fixed r, the optimal number of fractions follows a more complicated trend as α_2^τ increases when M_2 is the optimal modality. For some values of r, it first increases and then decreases, whereas for other values of r it decreases. The optimal number of fractions is independent of α_2^τ and r as expected, when M_1 is the optimal modality.

Table 1.5 shows the ratio of surviving cells when an optimal modality is used with an optimal number of fractions, relative to the standard practice of using M_1 with $N_{\text{conv}} = 25$ fractions (in contrast to Table 1.3 wherein the number of fractions is not optimized). As expected, the surviving cell ratios are lower in Table 1.5 than in Table 1.3. This is because (for the optimal modality) the number of fractions is optimized in Table 1.5 whereas it is fixed at $N_{\text{conv}} = 25$ in Table 1.3. All other qualitative trends regarding the choice of optimal modalities in Table 1.5 are identical to those in Table 1.3.

Finally, Table 1.6 shows the ratio of surviving cells when an optimal modality is used with an optimal number of fractions, relative to using M_1 with a number of fractions that is optimal for M_1 (contrast this with Tables 1.5 and 1.3). As expected, the surviving cell ratios are higher in Table 1.6 than in Table 1.5. This is because the number of fractions with M_1 is optimized in Table 1.6 but not in Table 1.5. All other qualitative trends regarding the choice of optimal modalities in Table 1.6 are identical to those in Table 1.5.

		Tumor alpha2									
		0.35	0.40	0.45	0.50	0.55	0.60	0.65	0.70	0.75	0.80
r	0.2	0.000	0.000	0.000	0.000	0.000	0.000	0.000	0.000	0.000	0.000
	0.4	0.003	0.000	0.000	0.000	0.000	0.000	0.000	0.000	0.000	0.000
	0.6	0.026	0.004	0.001	0.000	0.000	0.000	0.000	0.000	0.000	0.000
	0.8	0.178	0.037	0.009	0.002	0.001	0.000	0.000	0.000	0.000	0.000
	1.0	1.000	0.283	0.092	0.033	0.013	0.006	0.003	0.002	0.001	0.000
	1.2	1.000	1.000	0.701	0.322	0.162	0.089	0.052	0.033	0.022	0.015
	1.4	1.000	1.000	1.000	1.000	0.987	0.787	0.572	0.417	0.313	0.242
	1.6	1.000	1.000	1.000	1.000	1.000	1.000	1.000	1.000	0.998	0.960
	1.8	1.000	1.000	1.000	1.000	1.000	1.000	1.000	1.000	1.000	1.000

Table 1.3: Ratio of surviving cells attained by using an optimal modality (or combination) with $N_{\text{conv}} = 25$ fractions, relative to using M_1 with $N_{\text{conv}} = 25$ fractions.

		Tumor alpha2									
		0.35	0.40	0.45	0.50	0.55	0.60	0.65	0.70	0.75	0.80
r	0.2	66	77	87	95	102	108	113	116	119	121
	0.4	44	49	53	55	57	59	59	60	60	60
	0.6	32	35	36	37	38	38	38	38	37	37
	0.8	25	26	27	27	27	27	27	26	26	25
	1.0	20	20	21	21	21	20	20	20	19	19
	1.2	20	20	16	16	16	16	16	15	15	15
	1.4	20	20	20	20	13	13	13	12	12	12
	1.6	20	20	20	20	20	20	20	10	10	9
	1.8	20	20	20	20	20	20	20	20	20	20

Table 1.4: Optimal number of fractions and optimal modality.

1.3.2 Physically superior modality M_2 combined with conventional modality M_1

In this section, we investigate the case where M_2 is physically superior to M_1 as characterized by $s_2 < s_1 = 1$ (recall that we fix $s_1 = 1$ in all numerical experiments). The biological characteristics of M_2 are assumed to be similar to M_1 when $r = 1$. For example, this section therefore studies trade-offs between conventional photon EBRT and protons. Results are summarized in Tables 1.7-1.10 over the ranges of $0.2 - 1.8$ for r, and $1.0 - 0.75$ for s_2.

Table 1.7 shows the ratio of surviving cells when an optimal modality (or combination) is used with the total number of fractions fixed at $N_{\text{conv}} = 25$, relative to the standard

r \ Tumor alpha2	0.35	0.40	0.45	0.50	0.55	0.60	0.65	0.70	0.75	0.80
0.2	0.000	0.000	0.000	0.000	0.000	0.000	0.000	0.000	0.000	0.000
0.4	0.001	0.000	0.000	0.000	0.000	0.000	0.000	0.000	0.000	0.000
0.6	0.022	0.003	0.000	0.000	0.000	0.000	0.000	0.000	0.000	0.000
0.8	0.178	0.037	0.009	0.002	0.001	0.000	0.000	0.000	0.000	0.000
1.0	0.880	0.256	0.084	0.031	0.012	0.005	0.003	0.001	0.001	0.000
1.2	0.880	0.880	0.475	0.213	0.104	0.054	0.030	0.018	0.011	0.007
1.4	0.880	0.880	0.880	0.880	0.550	0.327	0.205	0.134	0.091	0.065
1.6	0.880	0.880	0.880	0.880	0.880	0.880	0.880	0.664	0.487	0.367
1.8	0.880	0.880	0.880	0.880	0.880	0.880	0.880	0.880	0.880	0.880

Table 1.5: Ratio of surviving cells attained by using an optimal modality with an optimal number of fractions, relative to using M_1 with $N_{\text{conv}} = 25$ fractions.

r \ Tumor alpha2	0.35	0.40	0.45	0.50	0.55	0.60	0.65	0.70	0.75	0.80
0.2	0.000	0.000	0.000	0.000	0.000	0.000	0.000	0.000	0.000	0.000
0.4	0.001	0.000	0.000	0.000	0.000	0.000	0.000	0.000	0.000	0.000
0.6	0.025	0.003	0.000	0.000	0.000	0.000	0.000	0.000	0.000	0.000
0.8	0.203	0.042	0.010	0.003	0.001	0.000	0.000	0.000	0.000	0.000
1.0	1.000	0.291	0.095	0.035	0.014	0.006	0.003	0.001	0.001	0.000
1.2	1.000	1.000	0.540	0.242	0.118	0.062	0.034	0.020	0.013	0.008
1.4	1.000	1.000	1.000	1.000	0.625	0.372	0.233	0.152	0.104	0.073
1.6	1.000	1.000	1.000	1.000	1.000	1.000	1.000	0.755	0.554	0.417
1.8	1.000	1.000	1.000	1.000	1.000	1.000	1.000	1.000	1.000	1.000

Table 1.6: Ratio of surviving cells attained by using an optimal modality with an optimal number of fractions, relative to using M_1 only with a number of fractions that is optimal for M_1.

practice of using M_1 with $N_{\text{conv}} = 25$ fractions. The table shows that for a fixed s_2, the optimal modality switches from M_2 to M_1 as r increases because the relative damage to the OAR from M_2 becomes larger, making M_2 less desirable. For a fixed r, the optimal modality switches from M_1 to M_2 because M_2 delivers less dose to the OAR (superior physical characteristics). Therefore, for sufficiently low fixed values of r, M_2 dominates M_1 for all values of s_2 because M_2 inflicts only a small damage on the OAR compared to the tumor.

Similarly, for sufficiently high values of r, M_1 or (M_1, M_2) dominates M_2 for all values of s_2. The switch from M_1 to M_2 occurs at lower values of s_2 as r increases. Similarly, the switch from M_2 to M_1 occurs at higher values of r as s_2 decreases. For each fixed value of s_2, the surviving cell ratio is nondecreasing as r increases because M_2 becomes less desirable. Similarly, for each fixed value of r, the surviving cell ratio is nonincreasing as s_2 decreases because M_2 becomes more desirable. The logic behind all these trends is qualitatively similar to that in Table 1.3.

Table 1.8 shows optimal modalities and the optimal number of fractions obtained by solving problem (P) (in contrast with Table 1.7 wherein the number of fractions is not optimized). The qualitative trends in the choice of optimal modality are identical to that in Table 1.7 as expected. Moreover, for each fixed s_2, the optimal number of fractions is nonincreasing as r increases when M_2 is the optimal modality. Again, this may be because as M_2 damages the OAR more and more relative to the tumor, prolonged fractionation is less desirable. For each fixed r, the optimal number of fractions seems to be nondecreasing as s_2 decreases when M_2 is the optimal modality. This may be because the damage to the OAR decreases as s_2 decreases and hence prolonged fractionation could be beneficial. The optimal number of fractions is independent of s_2 and r as expected, when M_1 is the optimal modality.

Table 1.9 shows the ratio of surviving cells when an optimal modality is used with an optimal number of fractions, relative to using M_1 with $N_{\text{conv}} = 25$ fractions (in contrast to Table 1.7 wherein the number of fractions is not optimized). As expected, the surviving cell ratios are lower in Table 1.9 than in Table 1.7. This is because (for the optimal modality) the number of fractions is optimized in Table 1.9 whereas it is fixed at $N_{\text{conv}} = 25$ in Table 1.7. All other qualitative trends regarding the choice of optimal modalities in Table 1.9 are identical to those in Table 1.7.

Finally, Table 1.10 shows the ratio of surviving cells when an optimal modality is used with an optimal number of fractions, relative to using M_1 with a number of fractions that is optimal with M_1 (contrast this with Tables 1.9 and 1.7). As expected, the surviving cell

ratios are higher in Table 1.10 than in Table 1.9. This is because the number of fractions with M_1 is optimized in Table 1.10 but not in Table 1.9. All other qualitative trends regarding the choice of optimal modalities in Table 1.10 are identical to those in Table 1.9.

		s2					
		1.00	0.95	0.90	0.85	0.80	0.75
r	0.2	0.000	0.000	0.000	0.000	0.000	0.000
	0.4	0.003	0.001	0.000	0.000	0.000	0.000
	0.6	0.026	0.006	0.001	0.000	0.000	0.000
	0.8	0.178	0.043	0.009	0.001	0.000	0.000
	1.0	1.000	0.273	0.063	0.012	0.002	0.000
	1.2	1.000	1.000	0.371	0.080	0.014	0.002
	1.4	1.000	1.000	1.000	0.445	0.089	0.014
	1.6	1.000	1.000	1.000	1.000	0.466	0.084
	1.8	1.000	1.000	1.000	1.000	1.000	0.417

Table 1.7: Ratio of surviving cells attained by using an optimal modality (or combination) with $N_{\text{conv}} = 25$ fractions, relative to using M_1 with $N_{\text{conv}} = 25$ fractions.

		s2					
		1.00	0.95	0.90	0.85	0.80	0.75
r	0.2	66	71	78	84	92	102
	0.4	44	47	51	54	59	63
	0.6	32	34	36	39	41	44
	0.8	25	26	27	29	31	32
	1.0	20	20	21	22	24	25
	1.2	20	20	17	18	19	19
	1.4	20	20	20	14	15	15
	1.6	20	20	20	12	12	12
	1.8	20	20	20	20	10	10

Table 1.8: Optimal number of fractions and optimal modality.

		s2					
		1.00	0.95	0.90	0.85	0.80	0.75
r	0.2	0.000	0.000	0.000	0.000	0.000	0.000
	0.4	0.001	0.000	0.000	0.000	0.000	0.000
	0.6	0.025	0.005	0.001	0.000	0.000	0.000
	0.8	0.203	0.049	0.010	0.002	0.000	0.000
	1.0	1.000	0.284	0.068	0.013	0.002	0.000
	1.2	1.000	1.000	0.313	0.071	0.013	0.002
	1.4	1.000	1.000	1.000	0.281	0.059	0.010
	1.6	1.000	1.000	1.000	0.866	0.205	0.038
	1.8	1.000	1.000	1.000	1.000	0.580	0.121

Table 1.9: Ratio of surviving cells attained by using an optimal modality with an optimal number of fractions, relative to using M_1 with $N_{\text{conv}} = 25$ fractions.

		s2					
		1.00	0.95	0.90	0.85	0.80	0.75
r	0.2	0.000	0.000	0.000	0.000	0.000	0.000
	0.4	0.001	0.000	0.000	0.000	0.000	0.000
	0.6	0.022	0.004	0.001	0.000	0.000	0.000
	0.8	0.178	0.043	0.009	0.001	0.000	0.000
	1.0	0.880	0.250	0.060	0.012	0.002	0.000
	1.2	0.880	0.880	0.275	0.063	0.011	0.002
	1.4	0.880	0.880	0.880	0.247	0.052	0.008
	1.6	0.880	0.880	0.880	0.762	0.180	0.034
	1.8	0.880	0.880	0.880	0.880	0.511	0.106

Table 1.10: Ratio of surviving cells attained by using an optimal modality with an optimal number of fractions, relative to using M_1 only with a number of fractions that is optimal for M_1.

1.4 Conclusions

We presented the first-ever mathematical formulation of the optimal fractionation problem with two modalities under the LQ dose-response model. We showed that KKT conditions for this formulation can be tackled by solving a quartic equation. Our numerical experiments ex-

plored the effect of varying, in a one-at-a-time manner, parameters that characterize physical and biological properties of the two modalities. The results of these experiments were consistent with clinical intuition. This at least partially validates our formulation and solution methodology.

Although we focused on the case of a single OAR for simplicity, our methodology can be extended to multiple OAR. To see this, consider a problem with M OAR. Its formulation would include M constraints similar to (1.2). At least one of these constraints must be active at an optimal solution. So, if there is exactly one constraint active at an optimal solution, we need to consider M different possibilities. Furthermore, at most two active constraints are needed to uniquely determine a (d_1, d_2) combination. There are $\binom{M}{2}$ ways in which we can have two active constraints. These observations suggest that a problem with M OAR can be solved by (i) solving M problems with one OAR each via the method presented in this chapter; (ii) solving $\binom{M}{2}$ quartic equations to uniquely identify additional candidate (d_1, d_2) pairs; and (iii) identifying and comparing all feasible (d_1, d_2) pairs derived from steps (i) and (ii).

Uncertainty in various problem parameters was not explicitly incorporated into our formulation. Effects of uncertainty were only indirectly studied via sensitivity analyses. The next chapter provides one modeling and solution approach for explicitly incorporating uncertainty in problem parameters.

Chapter 2

ROBUST MODALITY SELECTION

First recall the following nominal problem from Chapter 1.

$$\min_{N_1,d_1,N_2,d_2} e^{-N_1\alpha_1^\tau d_1 - N_1\beta_1^\tau (d_1)^2 - N_2\alpha_2^\tau d_2 - N_2\beta_2^\tau (d_2)^2 + \pi(N_1+N_2)} \tag{2.1}$$

$$N_1 s_{1m}\alpha_{1m}^\phi d_1 + N_1\beta_{1m}^\phi (s_{1m}d_1)^2 + N_2\alpha_{2m}^\phi d_2 + N_2\beta_{2m}^\phi (s_{2m}d_2)^2 \le B_m,\ m \in \mathcal{M}, \tag{2.2}$$

$$d_1 \ge 0, \tag{2.3}$$

$$d_2 \ge 0, \tag{2.4}$$

$$N_1 + N_2 \le N_{\max}, \tag{2.5}$$

$$0 \le N_1 \text{ integer}, \tag{2.6}$$

$$0 \le N_2 \text{ integer}. \tag{2.7}$$

Here, the M OAR are indexed by $m \in \mathcal{M} = \{1, 2, \ldots, M\}$). Note that the right hand side (RHS) of constraint (2.2) is defined as $B_m = N_{\text{conv}}\alpha_{1m}^\phi d_{\text{conv }m} + N_{\text{conv}}\beta_{1m}^\phi (d_{\text{conv }m})^2$. This, in turn, can be rewritten as $B_m = \alpha_{1m}D_m + \beta_{1m}D_m^2/N_{\text{conv}}$ by letting $D_m = N_{\text{conv}}d_{\text{conv }m}$ for brevity. As in Chapter 1, this problem can be converted into an equivalent maximization problem after taking the natural logarithm of the objective function. Moreover, as in Chapter 1, it suffices to develop methodology to solve the problem for each fixed (N_1, N_2) combination. This is because the best (N_1, N_2) combination can then be found simply by choosing from results for a finite number of possible combinations. Consequently, in this chapter, we refer

to the following optimization problem as the nominal problem.

$$\max_{d_1,d_2} \; N_1\alpha_1^\tau d_1 + N_1\beta_1^\tau (d_1)^2 + N_2\alpha_2^\tau d_2 + N_2\beta_2^\tau (d_2)^2 \tag{2.8}$$

$$N_1 s_{1m}\alpha_{1m}^\phi d_1 + N_1\beta_{1m}^\phi (s_{1m}d_1)^2 + N_2\alpha_{2m}^\phi d_2 + N_2\beta_{2m}^\phi (s_{2m}d_2)^2 \leq B_m, \; m \in \mathcal{M}, \tag{2.9}$$

$$d_1 \geq 0, \tag{2.10}$$

$$d_2 \geq 0. \tag{2.11}$$

This chapter focuses on a robust counterpart of this nominal formulation.

2.1 Problem formulation under interval uncertainty

As stated in Chapter 1, one limitation of the above nominal formulation is that it ignores the uncertainty in both biological and physical parameters of the model. For instance, the uncertainty in biological parameters such as α and β may be rooted in the treatment planner's lack of knowledge regarding their "true" values. The uncertainty in physical parameters such as the sparing factors s may be rooted in the treatment planner's inability to accurately predict the location of the Bragg peak (for protons) or the amount of dose delivered to the OAR by the linear accelerator (for photons). To address this concern, this chapter presents a robust counterpart of the above nominal formulation using an interval model of uncertainty. Interval models are common in the robust optimization literature partly because of their simplicity and their connection to statistical confidence intervals [8]. Use of such interval models is also consistent with the clinical literature, where estimated ranges of parameter values are often reported [62, 75]. Ajdari and Ghate [3] employed a similar interval uncertainty model for the fractionation problem with a single modality. This chapter presents an extension of their formulation and solution method to the modality selection problem.

The robust counterpart in this chapter assumes that the treatment planner is uncertain about the OAR sparing factors s_{1m}, s_{2m}, and the OAR parameters $\alpha_{1m}^\phi, \beta_{1m}^\phi, \alpha_{2m}^\phi, \beta_{2m}^\phi$. The treatment planner assumes, however, that these parameters belong to the intervals $R_{s_{1m}} = [s_{1m}^{\min}, s_{1m}^{\max}]$, $R_{s_{2m}} = [s_{2m}^{\min}, s_{2m}^{\max}]$ $R_{\alpha_{1m}} = [\alpha_{1m}^{\min}, \alpha_{1m}^{\max}]$, $R_{\beta_{1m}} = [\beta_{1m}^{\min}, \beta_{1m}^{\max}]$, $R_{\alpha_{2m}} = [\alpha_{2m}^{\min}, \alpha_{2m}^{\max}]$,

and $R_{\beta_{2m}} = [\beta_{2m}^{\min}, \beta_{2m}^{\max}]$. Pursuing standard philosophy of robust optimization, the treatment planner takes a worst-case view of the problem. That is, the treatment planner computes the best solution that will remain feasible irrespective of the true value of these parameters from these intervals. Note here that we have not modeled uncertainty in the tumor's dose-response parameters. This can, in fact, be done trivially by setting the tumor's parameters to their largest values in the uncertainty interval. It is therefore common to not model uncertainty in the objective function parameters in such robust optimization problems [3, 8].

The aforementioned ideas yield the following robust counterpart of the nominal problem (2.8)-(2.11):

$$\begin{aligned}
&\max_{d_1,d_2} \; N_1\alpha_1^\tau d_1 + N_1\beta_1^\tau (d_1)^2 + N_2\alpha_2^\tau d_2 + N_2\beta_2^\tau (d_2)^2 \\
&N_1\alpha_{1m}^\phi s_{1m} d_1 + N_1\beta_{1m}^\phi (s_{1m}d_1)^2 + N_2\alpha_{2m}^\phi s_{2m} d_2 + N_2\beta_{2m}^\phi (s_{2m}d_2)^2 \leq \alpha_{1m}^\phi D_m + \beta_{1m}^\phi D_m^2/N_{\text{conv}}; \\
&\forall s_{1m} \in R_{s_{1m}},\ \forall s_{2m} \in R_{s_{2m}},\ \forall \alpha_{1m} \in R_{\alpha_{1m}},\ \forall \beta_{1m} \in R_{\beta_{1m}},\ \forall \alpha_{2m} \in R_{\alpha_{2m}},\ \forall \beta_{2m} \in R_{\beta_{2m}}, \\
&\forall m \in M, \qquad (2.12) \\
&d_1 \geq 0, \\
&d_2 \geq 0.
\end{aligned}$$

After algebraic simplification, constraint (2.12) can be rewritten as

$$\begin{aligned}
&\alpha_{1m}^\phi (N_1 s_{1m} d_1 - D_m) + \beta_{1m}^\phi (N_1 s_{1m}^2 d_1^2 - D_m^2/N_{\text{conv}}) + N_2\alpha_{2m}^\phi s_{2m} d_2 + N_2\beta_{2m}^\phi s_{2m}^2 d_2^2 \leq 0; \\
&\forall s_{1m} \in R_{s_{1m}},\ \forall s_{2m} \in R_{s_{2m}},\ \forall \alpha_{1m} \in R_{\alpha_{1m}},\ \forall \beta_{1m} \in R_{\beta_{1m}},\ \forall \alpha_{2m} \in R_{\alpha_{2m}},\ \forall \beta_{2m} \in R_{\beta_{2m}}, \\
&\forall m \in M. \qquad (2.13)
\end{aligned}$$

Note that the above constraint in fact encapsulates an uncountably infinite number of constraints because the uncertainty intervals include uncountably infinite distinct parameter values. Thus, this constraint is computationally impossible to enforce as is. In this chapter, we show that this robust problem with an uncountably infinite number of constraints can instead be tackled by solving a finite number of subproblems each with a finite number of constraints. Details of this reformulation process are explained in the next section.

2.1.1 Solution method

The initial intuitive idea in our solution method is to identify bottleneck parameter values on the left hand side (LHS) of the constraint in question. This is easy to do for the third and the fourth terms, $N_2\alpha_{2m}s_{2m}d_2$ and $N_2\beta_{2m}s_{2m}^2d_2^2$, respectively. This is because the bottleneck parameter values equal their largest values (as the multipliers N_2d_2 and $N_2d_2^2$ are nonnegative). That is, $\alpha_{2m}^{\max}$, $\beta_{2m}^{\max}$ and $s_{2m}^{\max}$ for α_{2m}^{ϕ}, β_{2m}^{ϕ} and s_{2m}, respectively. Similarly, the bottleneck value for s_{1m} is also $s_{1m}^{\max}$. A similar idea does not work for the first and the second terms because the multipliers $(N_1s_{1m}^{\max}d_1 - D_m)$ and $(N_1(s_{1m}^{\max})^2d_1^2 - D_m^2/N_{\text{conv}})$ may be positive or negative. An alternative approach to handle these terms is therefore developed next.

Note that the sign of the multiplier $(N_1s_{1m}^{\max}d_1 - D_m)$ is determined by whether or not $d_1 \geq (D_m/N_1s_{1m}^{\max})$. If the sign is negative, then the largest value of the first term $\alpha_{1m}^{\phi}(N_1s_{1m}^{\max}d_1 - D_m)$ on the LHS of the constraint is attained when $\alpha_{1m}^{\phi} = \alpha_{1m}^{\min}$. On the other hand, if the sign is positive, then the largest value of the first term is attained when $\alpha_{1m}^{\phi} = \alpha_{1m}^{\max}$. Similarly, the sign of the multiplier $(N_1(s_{1m}^{\max})^2d_1^2 - D_m^2/N_{\text{conv}})$ is determined by whether or not $d_1^2 \geq (D_m^2/N_{\text{conv}}N_1(s_{1m}^{\max})^2)$. If the sign is negative, then the largest value of the second term $\beta_{1m}^{\phi}(N_1(s_{1m}^{\max})^2d_1^2 - D_m^2/N_{\text{conv}})$ is attained when $\beta_{1m}^{\phi} = \beta_{1m}^{\min}$. On the other hand, if the sign is positive, then the largest value of the second term is attained when $\beta_{1m}^{\phi} = \beta_{1m}^{\max}$. To exploit these observations in a streamlined manner, we sort the values $\mu_m = \frac{D_m}{N_1s_{1m}^{\max}}$ in increasing order and also sort the values $\nu_m = \frac{D_m^2}{N_{\text{conv}}N_1(s_{1m}^{\max})^2}$ in increasing order. The sorted OAR indices m are stored in sequences L and Q, respectively. Suppose that, for any $i = 1, 2, \ldots, M$, L_i denotes the ith OAR index in the sorted sequence L. Then $\mu_{L_i} \leq \mu_{L_{i+1}}$, for $i = 1, 2, \ldots, M-1$. Similarly, suppose that, for any $j = 1, 2, \ldots, M$, Q_j denotes the jth OAR index in the sorted sequence Q. Then $\nu_{Q_j} \leq \nu_{Q_{j+1}}$, for $j = 1, 2, \ldots, M-1$. We use this notation to partition the dose values $d_1 \geq 0$ that are feasible to (2.13) into different subsets. These subsets are indexed by pairs (ℓ, q), for $\ell \in \{0, 1, 2, \ldots, M\}$ and $q \in \{0, 1, 2, \ldots, M\}$.

The (ℓ, q)th subset is characterized by the scenario

$$d_1 \geq \mu_m \text{ for } m \in \{L_1, L_2, \ldots, L_\ell\} \text{ and } d_1 \leq \mu_m \text{ for } m \in \{L_{\ell+1}, L_{\ell+2}, \ldots, L_M\}; \text{ and}$$
$$d_1^2 \geq \nu_m \text{ for } m \in \{Q_1, Q_2, \ldots, Q_q\} \text{ and } d_1^2 \leq \nu_m \text{ for } m \in \{Q_{q+1}, Q_{q+2}, \ldots, Q_M\}.$$

This discussion implies that the robust problem can be tackled by instead solving a group of subproblems indexed by (ℓ, q) pairs, for $\ell \in \{0, 1, 2, \ldots, M\}$ and $q \in \{0, 1, 2, \ldots, M\}$, and then by identifying the (ℓ, q) pair and the corresponding (d_1, d_2) doses that yield the largest objective value. The (ℓ, q)th subproblem from this group is given by

$$\max_{d_1, d_2} \; N_1\alpha_1^\tau d_1 + N_1\beta_1^\tau (d_1)^2 + N_2\alpha_2^\tau d_2 + N_2\beta_2^\tau (d_2)^2 \tag{2.14}$$

$$\alpha_{1m}^{\max}(N_1 s_{1m}^{\max} d_1 - D_m) + \beta_{1m}^{\max}(N_1 (s_{1m}^{\max})^2 d_1^2 - D_m^2/N_{\text{conv}}) + N_2\alpha_{2m}^{\max} s_{2m}^{\max} d_2 + N_2\beta_{2m}^{\max}(s_{2m}^{\max})^2 d_2^2$$
$$\leq 0, \; m \in \{\{L_1, L_2, \ldots, L_\ell\} \cap \{Q_1, Q_2, \ldots, Q_q\}\}; \tag{2.15}$$

$$\alpha_{1m}^{\max}(N_1 s_{1m}^{\max} d_1 - D_m) + \beta_{1m}^{min}(N_1 (s_{2m}^{\max})^2 d_1^2 - D_m^2/N_{\text{conv}}) + N_2\alpha_{2m}^{\max} s_{2m}^{\max} d_2 + N_2\beta_{2m}^{\max}(s_{2m}^{\max})^2 d_2^2$$
$$\leq 0, \; m \in \{\{L_1, L_2, \ldots, L_\ell\} \cap \{Q_{q+1}, Q_{q+2}, \ldots, Q_M\}\}; \tag{2.16}$$

$$\alpha_{1m}^{min}(N_1 s_{1m}^{\max} d_1 - D_m) + \beta_{1m}^{min}(N_1 (s_{1m}^{\max})^2 d_1^2 - D_m^2/N_{\text{conv}}) + N_2\alpha_{2m}^{\max} s_{2m}^{\max} d_2 + N_2\beta_{2m}^{\max}(s_{2m}^{\max})^2 d_2^2$$
$$\leq 0, \; m \in \{\{L_{\ell+1}, L_{\ell+2}, \ldots, L_M\} \cap \{Q_{q+1}, Q_{q+2}, \ldots, Q_M\}\}; \tag{2.17}$$

$$\alpha_{1m}^{\min}(N_1 s_{1m}^{\max} d_1 - D_m) + \beta_{1m}^{\max}(N_1 (s_{1m}^{\max})^2 d_1^2 - D_m^2/N_{\text{conv}}) + N_2\alpha_{2m} s_{2m}^{\max} d_2 + N_2\beta_{2m}(s_{2m}^{\max})^2 d_2^2$$
$$\leq 0, \; m \in \{\{L_{\ell+1}, L_{\ell+2}, \ldots, L_M\} \cap \{Q_1, Q_2, \ldots, Q_q\}\}; \tag{2.18}$$

$$d_1 \geq \mu_m, \; m \in \{L_1, L_2, \ldots, L_\ell\}, \tag{2.19}$$

$$d_1 \leq \mu_m, \; m \in \{L_{\ell+1}, L_{\ell+2}, \ldots, L_M\}, \tag{2.20}$$

$$d_1^2 \geq \nu_m, \; m \in \{Q_1, Q_2, \ldots, Q_q\}, \tag{2.21}$$

$$d_1^2 \leq \nu_m, \; m \in \{Q_{q+1}, Q_{q+2}, \ldots, Q_M\}, \tag{2.22}$$

$$d_1 \geq 0, \tag{2.23}$$

$$d_2 \geq 0. \tag{2.24}$$

This subproblem includes M constraints in (2.15-2.18) and $2M$ constraints (2.19-2.22). This makes a total of $3M + 2$ constraints. Since there are $(M + 1)^2$ possible pairs (ℓ, q), we need

to solve $(M+1)^2$ such subproblems. Furthermore, each subproblem can be solved using a KKT approach similar to that in Chapter 1 as described next.

Since the above subproblem includes only two variables, it is sufficient to investigate two cases: whether only one or at least two constraints are active at an optimal solution. Because of the structure of our constraints, we categorize the constraints into three groups: (2.15-2.18); (2.19-2.22); and (2.23-2.24). Then we investigate the two cases for each category separately as follows.

1. Only one of the constraints (2.15-2.18) is active at optimal solution. Then, there are two possible subcases:

   (a) Only one of d_1 and d_2 is positive. Suppose $d_1 > 0$ and $d_2 = 0$. The (l, q) subproblem becomes a single modality problem with d_1 as the only variable. Then, by making constraints (2.15-2.18) active one-by-one, we are able to obtain a positive value of d_1 by solving a quadratic equation. Among all such candidate values of d_1, we only keep those that are feasible to the rest of the constraints in (2.15-2.18), as well as in (2.19-2.22). The same approach can be repeated when $d_1 = 0$ and $d_2 > 0$.

   (b) Both $d_1 > 0$ and $d_2 > 0$. We assume each one of the constraints (2.15-2.18) to be active one-by-one and the rest of them to be strict inequalities. Thus there will be M subcases to consider. In each of the subcases, the Lagrange multipliers for the $M-1$ inactive constraints among (2.15-2.18), for the $2M$ inactive constraints (2.19-2.22), and also for the two non-negativity constraints (2.23-2.24) become zero owing to complementary slackness. Thus, the KKT conditions reduce to those identical to the two-modality and single constraint problem with $d_1 > 0$ and $d_2 > 0$ in Chapter 1. After solving these KKT conditions for each of the aforementioned problems, we only keep solutions that are feasible to the original subproblem.

2. At least two of the constraints (2.15-2.18) are active at optimal solution. As the problem includes two variables, the active constraints will provide a system of two quadratic equations that can be easily solved for d_1 and d_2. In particular, the intersection of the two active constraints creates a quartic equation in terms of either d_1 or d_2, which can be solved in closed form. Then by substituting the obtained d_1 or d_2 in either of the constraints, we get a quadratic equation with one unknown variable, which also can be easily solved in closed from. There will be $\binom{M}{2}$ such systems of two quadratic equations. From the resulting candidate solutions, we keep the ones that are feasible for the entire subproblem.

3. At least one of the constraints (2.19-2.22) is active. In this case, we make each of the constraints (2.19-2.22) active one-at-a-time and solve it for d_1. Then we substitute the resulting value of d_1 into constraints (2.15-2.18). Note that at least one of the constraints (2.15-2.18) must then be active at optimal solution, because the objective function is increasing in d_2. Thus we solve M quadratic equations one-by-one to obtain candidate solutions for d_2. Among, the resulting solutions, we only keep the (d_1, d_2) pairs that are feasible for the entire suproblem.

The above three cases yield a finite set of feasible solutions for the (l, q) subproblem, and this set contains an optimal solution to that problem. Thus, an optimal solution to the subproblem can be identified by comparing objective values of these candidate solutions. By repeating this process for every subproblem, and then identifying the subproblem that yields a solution with the best objective value, we are able to solve the original robust problem.

2.2 Numerical results

Our numerical results are categorized into two parts that are presented in Sections 2.2.1 and 2.2.2. Section 2.2.1 studies the effect of uncertainty in the physical characteristics (s_2) of M_2. Section 2.2.2 investigates uncertainty in the biological power (α_1^{ϕ}) of M_1. As in Chapter 1,

$\alpha_1^\tau = 0.35$ Gy^{-1}	$\beta_1^\tau = 0.035$ Gy^{-2}
$\alpha_1^\phi = 0.35$ Gy^{-1}	$\beta_1^\phi = 0.175$ Gy^{-2}

Table 2.1: Parameters for modality M_1.

we pursue this one-at-a-time method of performing sensitivity analyses because it facilitates interpretation of results.

As in 1, both Sections 2.2.1 and 2.2.2 include results for different values of a biological parameter $r = \alpha_2^\phi/\alpha_2^\tau$. Recall the following thought process about this parameter from 1. A biologically superior modality will inflict a higher damage on both the tumor and the OAR. The ratio r attempts to capture the differential in the damage to the tumor and the OAR. As r increases, the damage to the OAR relative to the damage to the tumor using M_2 increases, when all other things are equal. Thus, M_2 becomes less desirable as r increases.

The base-case values for both modalities were identical to those in 1. In particular, for the conventional modality M_1, we used $s_1 = 1$ as the base-value of physical characteristics. Also, for M_1, we used $\alpha_1^\tau/\beta_1^\tau = 10$ Gy, $\alpha_1^\phi/\beta_1^\phi = 2$ Gy, and the OAR tolerance was assumed to be $N_{\text{conv}}d_{\text{conv}} = 50$ Gy delivered in $N_{\text{conv}} = 25$ fractions [31, 49]. Table 2.1 shows other specific parameter values for M_1. These values are standard in the clinical literature [22, 23, 31, 49], and yield $B = 35$ as the right hand side of constraint (1.2) in the base case as in Chapter 1. Similarly, β_2^ϕ was fixed at 0.175 Gy^{-2} and β_2^τ was fixed at 0.035 Gy^{-2} throughout this chapter.

We used formula (1.24) from Chapter 1 for the tumor repopulation term $\pi(N_1 + N_2)$. We present results with $T_d = 3$ days and $T_{\text{lag}} = 0$ day as representative values since qualitative trends in our results were invariant with respect to these numbers. We fixed $N_{\max}$ at 50 days throughout.

2.2.1 Uncertainty in physical characteristic of M_2

In this section, we study the effect of uncertainty in s_2, which is viewed in this chapter as a physical characteristic of M_2. All other problem parameters are assumed to be known with certainty. For example, for protons, this could model the uncertainty in the location of the Bragg peak. The uncertainty interval $[s_2^{\min}, s_2^{\max}]$ is modeled by setting $s_2^{\min} = (1-\Delta)s_2$ and $s_2^{\max} = (1+\Delta)s_2$, for $\Delta \in \{0, 0.1, 0.2, \ldots, 0.9\}$. Here, s_2 is a nominal value chosen from the set $\{1, 0.9, \ldots, 0.5\}$, and $\Delta = 0$ corresponds to the case of no uncertainty, that is, the nominal case.

Tables 2.2-2.4 report results for $r = 1$, $r = 0.8$, and $r = 1.2$, respectively. Each row of each table considers a different nominal value of s_2. Different columns correspond to different levels of uncertainty Δ. The tables report the % price of robustness for each (s_2, Δ) combination. For each row (that is, for each nominal value of s_2), this is defined as the percentage increase in the optimal number of surviving cells in the robust formulation (where $\Delta \geq 0$) relative to the optimal number of surviving cells in the nominal formulation (where $\Delta = 0$). Tables are colored following the same scheme as in Table 1.1 from Chapter 1.

Table 2.2 shows that for each fixed s_2 (that is, in each row), the price of robustness is nondecreasing as Δ increases. When Δ increases, $s_2^{\max}$ increases and M_2 becomes less desirable as M_2 inflicts more damage on the OAR. The optimal modality thus switches to M_1 at a sufficiently high value of Δ. After this switch occurs, the optimal solution does not depend on parameters of M_2, and in particular, does not depend on Δ. Thus, the price of robustness is constant for all values of Δ where M_1 is optimal in each row. In the top-left cell where $s_2 = 1$ and $\Delta = 0$, M_1 and M_2 are equivalent. Therefore, there is a tie between M_1 and M_2 in that cell. In particular, since the price of robustness is 0 in that cell, it remains 0 throughout that row of $s_2 = 1$ (note that the price of robustness is always 0 as expected when $\Delta = 0$). As the nominal value of s_2 decreases from 1.0 to 0.5, M_2 becomes more desirable because it inflicts less damage on the OAR. Thus, the switch from M_2 to M_1

in each row occurs at a larger value of Δ. Similarly, for each fixed value of Δ, M_2 becomes more desirable as the nominal s_2 decreases. The optimal modality thus switches from M_1 to M_2. This switch occurs at smaller and smaller values of nominal s_2 as Δ increases (because higher Δs make M_2 less desirable whereas lower s_2s make it more desirable). For each fixed value of Δ, the price of robustness increases as s_2 decreases, whenever M_1 is optimal. This is because the number of surviving cells with M_1 as the optimal modality is invariant as a function of s_2 in this situation, but the number of surviving cells with M_2 as the optimal modality in the nominal problem ($\Delta = 0$) is decreasing as s_2 decreases.

		Uncertainty Δ									
		0.0	0.1	0.2	0.3	0.4	0.5	0.6	0.7	0.8	0.9
nominal s_2	1.00	0.0	0.0	0.0	0.0	0.0	0.0	0.0	0.0	0.0	0.0
	0.90	0.0	13.4	14.7	14.7	14.7	14.7	14.7	14.7	14.7	14.7
	0.80	0.0	13.3	24.0	28.5	28.5	28.5	28.5	28.5	28.5	28.5
	0.70	0.0	13.2	23.8	32.4	39.6	41.4	41.4	41.4	41.4	41.4
	0.60	0.0	13.1	23.6	32.2	39.3	45.3	50.3	53.3	53.3	53.3
	0.50	0.0	13.0	23.4	31.9	39.0	44.9	50.0	54.3	58.1	61.4

Table 2.2: Price of robustness (%) attained by using an optimal modality (or combination) and optimal number of fractions, with $r = 1$. Here, the two modalities have identical properties in the absence of uncertainty at the base case (that is, when $s_2 = 1$, $\Delta = 0$).

The qualitative trends in Table 2.3 are identical to those in Table 2.2. However, M_2 is optimal in more cells in Table 2.3 than in Table 2.2. This is because Table 2.3 uses a smaller value of $r = 0.8$ as compared to Table 2.2 where $r = 1$. This means that M_2 causes less damage to the OAR in the former and hence it is more desirable. It is for this same reason that in each fixed row of Table 2.3, the switch from M_2 to M_1 occurs at a higher value of Δ than that in Table 2.2. Similarly, for each fixed column of Table 2.3, the switch from M_1 to M_2 occurs at a higher value of s_2 than that in Table 2.2.

The qualitative trends in Table 2.4 are also identical to those in Table 2.2. However, M_2 is optimal in fewer cells in Table 2.4 than in Table 2.2. This is because Table 2.3 uses a

nominal s_2 \ Uncertainty Δ	0.0	0.1	0.2	0.3	0.4	0.5	0.6	0.7	0.8	0.9
1.00	0.0	13.1	21.5	21.5	21.5	21.5	21.5	21.5	21.5	21.5
0.90	0.0	13.0	23.5	32.1	32.7	32.7	32.7	32.7	32.7	32.7
0.80	0.0	12.9	23.3	31.8	38.9	43.3	43.3	43.3	43.3	43.3
0.70	0.0	12.8	23.1	31.5	38.6	44.5	49.6	53.2	53.2	53.2
0.60	0.0	12.6	22.9	31.2	38.2	44.1	49.2	53.5	57.3	60.6
0.50	0.0	12.5	22.6	30.9	37.8	43.7	48.7	53.0	56.8	60.0

Table 2.3: Price of robustness (%) attained by using an optimal modality (or combination) and optimal number of fractions, with $r = 0.8$. Here, M_2 is biologically superior to M_1 in the absence of uncertainty at the base case (that is, when $s_2 = 1$, $\Delta = 0$).

higher value of $r = 1.2$ as compared to Table 2.2 where $r = 1$. This means that M_2 causes more damage to the OAR in the former and hence it is less desirable. It is for this same reason that in each fixed row of Table 2.4, the switch from M_2 to M_1 occurs at a lower value of Δ than that in Table 2.2. Similarly, for each fixed column of Table 2.3, the switch from M_1 to M_2 occurs at a lower value of s_2 than that in Table 2.2.

nominal s_2 \ Uncertainty Δ	0.0	0.1	0.2	0.3	0.4	0.5	0.6	0.7	0.8	0.9
1.00	0.0	0.0	0.0	0.0	0.0	0.0	0.0	0.0	0.0	0.0
0.90	0.0	0.0	0.0	0.0	0.0	0.0	0.0	0.0	0.0	0.0
0.80	0.0	13.7	15.3	15.3	15.3	15.3	15.3	15.3	15.3	15.3
0.70	0.0	13.6	24.4	31.0	31.0	31.0	31.0	31.0	31.0	31.0
0.60	0.0	13.5	24.3	33.0	40.2	45.5	45.5	45.5	45.5	45.5
0.50	0.0	13.5	24.2	32.9	40.0	46.1	51.2	55.5	58.6	58.6

Table 2.4: Price of robustness (%) attained by using an optimal modality (or combination) and optimal number of fractions, with $r = 1.2$. Here, M_1 is biologically superior to M_2 in the absence of uncertainty at the base case (that is, when $s_2 = 1$, $\Delta = 0$).

2.2.2 Uncertainty in biological characteristic of M_1

In this section, we study the effect of uncertainty in α_1^ϕ, which is viewed in this chapter as a biological characteristic of M_1. All other problem parameters are assumed to be known with certainty. For example, for the conventional modality of photons, this could model the uncertainty in its biological power (see [24, 83]). The uncertainty interval $[\alpha_1^{\min}, \alpha_1^{\max}]$ is modeled by setting $\alpha_1^{\min} = (1-\Delta)\alpha_1^\phi$ and $\alpha_1^{\max} = (1+\Delta)\alpha_1^\phi$, for $\Delta \in \{0, 0.1, 0.2, \ldots, 0.9\}$. Here, the nominal value α_1^ϕ is fixed at 0.35 Gy^{-1}. Recall that $\Delta = 0$ corresponds to the case of no uncertainty.

Tables 2.5-2.7 report results for $r = 1$, $r = 0.8$, and $r = 1.2$, respectively. Each row of each table considers a different nominal value of α_2^τ, which models the biological power of M_2. Different columns correspond to different levels of uncertainty Δ. The tables report the % price of robustness for each (α_2^τ, Δ) combination. For each row (that is, for each value of α_2^τ), this is defined as the percentage increase in the optimal number of surviving cells in the robust formulation (where $\Delta \geq 0$) relative to the optimal number of surviving cells in the nominal formulation (where $\Delta = 0$). Tables are colored following the same scheme as in Table 1.1 from Chapter 1. Qualitative trends in these three tables are harder to explain than those in the tables in Section 2.2.1. This is because, unlike s_2, uncertainty in α_1^ϕ affects both the LHS and the RHS of the OAR constraint.

Table 2.5 shows that for each fixed α_2^τ (that is, in each row), the price of robustness is nondecreasing as Δ increases. In each row, the price of robustness becomes constant after a sufficiently high value of Δ. A closer investigation of optimal doses revealed that at a sufficiently high value of Δ, dose d_1 reaches the value $D_1/N_1 s_{11}^{\max}$ and this eliminates the effect of uncertainty in α_1^ϕ from the OAR constraints. The price of robustness thus remains constant thereafter. Also, in each row, the optimal modality switches to M_1 (or a combination of M_1, M_2) as Δ increases. This fact that M_1 becomes more desirable as the uncertainty in its biological power increases may appear counterintuitive at first. However,

alpha^\tau_2 \ Uncertainty Δ in alpha_\phi1	0.0	0.1	0.2	0.3	0.4	0.5	0.6	0.7	0.8	0.9
0.35	0.0	0.4	0.6	0.8	0.8	0.8	0.8	0.8	0.8	0.8
0.40	0.0	4.9	7.9	8.1	8.1	8.1	8.1	8.1	8.1	8.1
0.45	0.0	4.9	9.9	13.8	13.8	13.8	13.8	13.8	13.8	13.8
0.50	0.0	4.9	9.9	14.8	18.4	18.4	18.4	18.4	18.4	18.4
0.55	0.0	4.9	9.9	14.8	19.8	22.2	22.2	22.2	22.2	22.2
0.60	0.0	4.9	9.9	14.8	19.8	24.7	25.1	25.1	25.1	25.1
0.65	0.0	4.9	9.9	14.8	19.8	24.7	27.6	27.6	27.6	27.6
0.70	0.0	4.9	9.9	14.8	19.8	24.7	29.6	29.7	29.7	29.7

Table 2.5: Price of robustness (%) attained by using an optimal modality (or combination) and optimal number of fractions, with $r = 1$. Here, the two modalities have identical properties in the absence of uncertainty at the base case (that is, when $\alpha_2^\tau = 0.35$ Gy^{-1} and $\Delta = 0$).

alpha^\tau_2 \ Uncertainty Δ in alpha_\phi1	0.0	0.1	0.2	0.3	0.4	0.5	0.6	0.7	0.8	0.9
0.35	0.0	4.9	9.9	10.0	10.0	10.0	10.0	10.0	10.0	10.0
0.40	0.0	4.9	9.9	14.8	17.6	17.6	17.6	17.6	17.6	17.6
0.45	0.0	4.9	9.9	14.8	19.8	23.4	23.4	23.4	23.4	23.4
0.50	0.0	4.9	9.9	14.8	19.8	24.7	27.8	27.8	27.8	27.8
0.55	0.0	4.9	9.9	14.8	19.8	24.8	29.7	31.3	31.3	31.3
0.60	0.0	5.0	9.9	14.9	19.8	24.8	29.7	34.1	34.1	34.1
0.65	0.0	5.0	9.9	14.9	19.8	24.8	29.7	34.7	36.4	36.4
0.70	0.0	5.0	9.9	14.9	19.8	24.8	29.7	34.7	38.3	38.3

Table 2.6: Price of robustness (%) attained by using an optimal modality (or combination) and optimal number of fractions, with $r = 0.8$. Here, M_2 is biologically superior to M_1 in the absence of uncertainty at the base case (that is, when $\alpha_2^\tau = 0.35$ Gy^{-1} and $\Delta = 0$).

this scenario is indeed possible, again because the uncertainty in α_1^ϕ affects both the LHS and the RHS of the OAR constraint. To test this conjecture, we artificially removed the dependence of the RHS $\alpha_1^\phi D_1 + \beta_1^\phi D_1^2/N_{\text{conv}}$ on α_1^ϕ by setting this RHS to a fixed constant. We then re-solved the problem. As expected, the optimal modality then did not switch from M_2 to M_1 in any row as Δ increased. For each fixed value of Δ (that is, in each column), the optimal modality switches from M_1 to M_2 (or a combination of M_1, M_2). This is because M_2 becomes more desirable as its α_2^τ (biological power) increases. For each fixed value of Δ, the

alpha^\tau_2 \ Uncertainty Δ in alpha_\phi1	0.0	0.1	0.2	0.3	0.4	0.5	0.6	0.7	0.8	0.9
0.35	0.0	0.4	0.6	0.8	0.8	0.8	0.8	0.8	0.8	0.8
0.40	0.0	0.4	0.6	0.8	0.8	0.8	0.8	0.8	0.8	0.8
0.45	0.0	4.2	4.4	4.6	4.6	4.6	4.6	4.6	4.6	4.6
0.50	0.0	4.9	8.9	9.1	9.1	9.1	9.1	9.1	9.1	9.1
0.55	0.0	4.9	9.9	12.8	12.8	12.8	12.8	12.8	12.8	12.8
0.60	0.0	4.9	9.9	14.8	15.9	15.9	15.9	15.9	15.9	15.9
0.65	0.0	4.9	9.9	14.8	18.5	18.5	18.5	18.5	18.5	18.5
0.70	0.0	4.9	9.9	14.8	19.8	20.7	20.7	20.7	20.7	20.7

Table 2.7: Price of robustness (%) attained by using an optimal modality (or combination) and optimal number of fractions, with $r = 1.2$. Here, M_1 is biologically superior to M_2 in the absence of uncertainty at the base case (that is, when $\alpha_2^\tau = 0.35$ Gy^{-1} and $\Delta = 0$).

price of robustness increases with α_2^τ as long as M_1 (or a combination of M_1, M_2) remains optimal. This is because, by continuing to use M_1, we are forgoing a better-quality M_2 as the biological power of M_2 increases.

The qualitative trends in Table 2.6 ($r = 0.8$) are identical to those in Table 2.5 ($r = 1$). But modality M_2 is biologically superior to modality M_1 in Table 2.6 because M_2 causes less damage to the OAR owing to a smaller value of r in the base case (that is, when $\alpha_2^\tau = 0.35$ Gy^{-1} and $\Delta = 0$). Thus, modality M_2 is optimal more frequently in Table 2.6. Consider any fixed (α_2^τ, Δ) pair where modality M_1 is optimal in both Tables 2.5 and 2.6 (either by itself or in combination with M_2). Then, the price of robustness in Table 2.6 is higher than that in Table 2.5. This is because, by utilizing M_1, we are forgoing a better-quality M_2 in Table 2.6.

The qualitative trends in Table 2.7 ($r = 1.2$) are identical to those in Table 2.5 ($r = 1$). But modality M_2 is biologically inferior to modality M_1 in Table 2.7 because M_2 causes more damage to the OAR owing to a larger value of r in the base case (that is, when $\alpha_2^\tau = 0.35$ Gy^{-1} and $\Delta = 0$). Thus, modality M_2 is optimal less frequently in Table 2.7. Consider any fixed (α_2^τ, Δ) pair where modality M_1 is optimal in both Tables 2.5 and 2.7 (either by itself or in combination with M_2). Then, the price of robustness in Table 2.7 is lower than that in

Table 2.5. This is because, by utilizing M_1, we are forgoing a lower-quality M_2 in Table 2.7.

2.3 Conclusions

This chapter investigated the effect of uncertainty in biological and physical characteristics of EBRT modalities on the choice of modality via a robust extension of the formulation in Chapter 1. We showed the solution of this robust formulation is analytically tractable, by equivalently partitioning the infinite-dimensional robust counterpart into a finite number of subproblems. Each subproblem can be solved via a KKT approach similar to Chapter 1. We performed numerical sensitivity analyses to gain insights into how uncertainty affects the choice of modality and the price of robustness. These insights matched with clinical intuition in scenarios where such intuition is easy to develop. We were also able to explain the less intuitive trends in our sensitivity analyses by a more careful investigation of the structure of constraints in the modality selection problem. These numerical results thus partly validate our robust formulation and solution method.

As is known in the literature, robust optimization takes a worst-case approach to uncertainty. This may be viewed as perhaps too conservative. The degree of conservatism was controlled by the parameter Δ in our numerical experiments. It may be interesting for other researchers to pursue alternative approaches in the future to tackle uncertainty in biological and physical properties of EBRT modalities.

The next chapter focuses on a spatiotemporally integrated formulation of the optimal modality selection problem, where, rather than optimizing doses d_1 and d_2, we directly optimize fluence-map vectors $u^{(1)}$ and $u^{(2)}$.

Chapter 3

SPATIOTEMPORALLY INTEGRATED OPTIMAL MODALITY SELECTION

In this chapter, we focus on extending the spatiotemporally separated model in Chapter 1 to a spatiotemporally integrated one. This essentially means that instead of assuming that the radiation intensity profiles for modalities M_1 and M_2 are available to the treatment planner and hence that it suffices to employ scalar dose variables d_1 and d_2, we directly optimize the radiation intensity profiles. This yielded a higher-dimensional nonconvex QCQP for modality selection. A simple approximate solution method rooted in convex programming is developed. Preliminary numerical results are presented as proof of concept for our problem formulation and solution method.

3.1 Problem formulation

Let K_1 and K_2 denote the number of beamlets in the radiation fields for modalities M_1 and M_2, respectively. Let $u^{(1)} \in \Re_+^{K_1}$ and $u^{(2)} \in \Re_+^{K_2}$ be the corresponding beamlet intensity vectors (also called fluence-maps). The set of OAR is given by $\mathcal{L} = \mathcal{L}_1 \cup \mathcal{L}_2$, where $\mathcal{L}_1$ is the set of serial OAR with maximum dose constraints, and $\mathcal{L}_2$ is the set of parallel OAR with mean dose constraints. For simplicity, and is in [42, 43], we do not include parallel OAR with dose-volume constraints in this chapter; they can be handled by using the constraint generation approach described for the single modality case in [69]. The voxels in OAR $\ell \in \mathcal{L}$ are indexed by $j = 1, 2, \ldots, L_\ell$. Let $A^{\ell,i}$ denote the $L_\ell \times K_i$ nonnegative dose-deposition matrix for OAR $\ell \in \mathcal{L}$ and modality i. That is, if fluence-map $u^{(i)}$ is used for modality i, then the dose deposited by modality i in the jth voxel of OAR ℓ is given by $A_j^{\ell,i} u^{(i)}$. Here, $A_j^{\ell,i}$ is the jth row of the dose-deposition matrix. Similarly, let $A^{(i)}$ denote the dose-deposition

matrix for the tumor. The tumor is assumed to include n voxels. Thus, if fluence-map $u^{(i)}$ is used for modality i, then the dose deposited by that modality in voxel j of the tumor is given by $A_j u^{(i)}$. Then the average dose delivered to the tumor via modality i is given by $\sum_{j=1}^{n} A_j u^{(i)}/n = \left(\sum_{j=1}^{n} A_j/n\right) u^{(i)} = \bar{A}^{(i)} u^{(i)}$. Here, we have defined $\bar{A}^{(i)} = \sum_{j=1}^{n} A_j/n$. We maximize the total BE of average doses administered by M_1 and M_2 to the tumor. The idea of maximizing the BE of average dose was originally employed in [69]. We follow that approach here. Other alternatives such as maximizing the minimum total BE administered over all voxels of the tumor can also pursued using our methodology. We refer the reader to [69] for pros and cons of such alternative objective functions. Suppose, for each $\ell \in \mathcal{L}_1$, that a dose $d_{\max}$ per fraction is known to be tolerated by each voxel in the serial OAR ℓ, if it is administered via the conventional modality M_1 in N^{ℓ}_{conv} equal-dose fractions. The BE of this conventional schedule equals

$$\text{BE}^{\ell}_{\max} = N^{\ell}_{\text{conv}} \alpha_1^{\phi_\ell} d_{\max} + N^{\ell}_{\text{conv}} \beta_1^{\phi_\ell} (d_{\max})^2. \tag{3.1}$$

Similarly, for each $\ell \in \mathcal{L}_1$, that a dose $d_{\max}$ per fraction is known to be tolerated by each voxel in the serial OAR ℓ, if it is administered via the conventional modality M_1 in N^{ℓ}_{conv} equal-dose fractions. The BE of this conventional schedule equals

$$\text{BE}^{\ell}_{\text{mean}} = N^{\ell}_{\text{conv}} \alpha_1^{\phi_\ell} d_{\text{mean}} + N^{\ell}_{\text{conv}} \beta_1^{\phi_\ell} (d_{\text{mean}})^2. \tag{3.2}$$

Then, we formulate the spatiotemporally integrated modality selection problem as

$$\max_{N_1,N_2,u^{(1)},u^{(2)}} \sum_{i=1}^{2} \left[N_i \alpha_i^\tau \bar{A}^{(i)} u^{(i)} + N_i \beta_i^\tau \left(\bar{A}^{(i)} u^{(i)} \right)^2 \right] - \pi(N_1 + N_2) \tag{3.3}$$

$$\sum_{i=1}^{2} \left(N_i \alpha_i^{\phi_\ell} (A_j^{\ell,i} u^{(i)}) + N_i \beta_i^{\phi_\ell} (A_j^{\ell,i} u^{(i)})^2 \right) \leq \mathrm{BE}_{\max}^{\ell},\ j = 1, \ldots, L_\ell,\ \ell \in \mathcal{L}_1, \tag{3.4}$$

$$\sum_{i=1}^{2} \left[N_i \alpha_i^{\phi_\ell} \left(\sum_{j=1}^{L_\ell} (A_j^{\ell,i} u^{(i)}) \right) + N_i \beta_i^{\phi_\ell} \left(\sum_{j=1}^{L_\ell} (A_j^{\ell,i} u^{(i)})^2 \right) \right] \leq L_\ell \mathrm{BE}_{\mathrm{mean}}^{\ell},\ \ell \in \mathcal{L}_2, \tag{3.5}$$

$$u^{(1)} \geq 0, \tag{3.6}$$

$$u^{(2)} \geq 0, \tag{3.7}$$

$$N_1 \geq 0,\ \text{integer}, \tag{3.8}$$

$$N_2 \geq 0,\ \text{integer}, \tag{3.9}$$

$$1 \leq N_1 + N_2 \leq N_{\max}. \tag{3.10}$$

Here, constraint (3.4) ensures that the total BE on every voxel in each serial OAR remains below the conventional BE. Similarly, constraint (3.5) ensures that the total mean BE on each parallel OAR remains below the conventional BE. Other constraints such as smoothness constraints on fluence-map can be easily incorporated into this formulation exactly as in [69]. They are omitted here for simplicity as they are not the main focus of this research.

3.2 Solution method

As in Chapter 1, it suffices to solve the above problem for each fixed nonnegative integer pair (N_1, N_2) such that $1 \leq N_1 + N_2 \leq N_{\max}$. We therefore consider the problem

$$(P) \max_{u^{(1)},u^{(2)}} \sum_{i=1}^{2} \left[N_i \alpha_i^\tau \bar{A}^{(i)} u^{(i)} + N_i \beta_i^\tau \left(\bar{A}^{(i)} u^{(i)} \right)^2 \right] \tag{3.11}$$

$$\sum_{i=1}^{2} \left(N_i \alpha_i^{\phi_\ell} (A_j^{\ell,i} u^{(i)}) + N_i \beta_i^{\phi_\ell} (A_j^{\ell,i} u^{(i)})^2 \right) \leq \mathrm{BE}_{\max}^{\ell},\ j = 1, \ldots, L_\ell,\ \ell \in \mathcal{L}_1, \tag{3.12}$$

$$\sum_{i=1}^{2} \left[N_i \alpha_i^{\phi_\ell} \left(\sum_{j=1}^{L_\ell} (A_j^{\ell,i} u^{(i)}) \right) + N_i \beta_i^{\phi_\ell} \left(\sum_{j=1}^{L_\ell} (A_j^{\ell,i} u^{(i)})^2 \right) \right] \leq L_\ell \mathrm{BE}_{\mathrm{mean}}^{\ell},\ \ell \in \mathcal{L}_2, \tag{3.13}$$

$$u^{(1)} \geq 0, \tag{3.14}$$

$$u^{(2)} \geq 0. \tag{3.15}$$

Note that we have dropped the constant term $\pi(N_1+N_2)$ from the objective function without loss of optimality.

It is easy to see that the feasible region of this problem is convex. The objective function is also convex; but since this is a maximization problem, this objective renders it nonconvex. In particular, this is a convex quadratically constrained problem with nonconvex quadratic objective. As such, it belongs to the class of nonconvex QCQPs. This class is NP-hard [47]. A number of approximate solution methods rooted in convex programming have been devised for nonconvex QCQPs over the last decade, and these problems continue to be an active area of research. The reader is referred to [60] for a survey written within the last six months. Rather than relying on these sophisticated generic approximation methods, we propose a slightly crude but simple approach that exploits the structure of our problem as described next.

First recall from [69] that in the single modality context, the nonconvex objective in the above problem can be linearized. As an example, suppose $N_2 = 0$, and thus consider the resulting single modality problem. The feasible region of course remains convex, but the objective is equivalent to simply maximizing $\bar{A}^{(1)} u^{(1)}$. Thus, the single modality problem

can be reformulated as one with a linear objective and convex quadratic constraints. In fact, recall from [69] that in the single modality case, constraints (3.12) can also be linearized by solving a quadratic equation after noting that the LHS is monotonic in the nonnegative number $A_j^{\ell,1}u^{(1)}$. Neither of these observations hold true in the case of two modalities. We partially remedy the first hurdle as described next.

We first equivalently rewrite the above problem as

$$\max_{u^{(1)},u^{(2)}} \quad t \tag{3.16}$$

$$\sum_{i=1}^{2}\left[N_i\alpha_i^\tau \bar{A}^{(i)}u^{(i)} + N_i\beta_i^\tau\left(\bar{A}^{(i)}u^{(i)}\right)^2\right] \geq t, \tag{3.17}$$

$$\sum_{i=1}^{2}\left(N_i\alpha_i^{\phi_\ell}(A_j^{\ell,i}u^{(i)}) + N_i\beta_i^{\phi_\ell}(A_j^{\ell,i}u^{(i)})^2\right) \leq \mathrm{BE}_{\max}^{\ell},\ j=1,\ldots,L_\ell,\ \ell\in\mathcal{L}_1, \tag{3.18}$$

$$\sum_{i=1}^{2}\left[N_i\alpha_i^{\phi_\ell}\left(\sum_{j=1}^{L_\ell}(A_j^{\ell,i}u^{(i)})\right) + N_i\beta_i^{\phi_\ell}\left(\sum_{j=1}^{L_\ell}(A_j^{\ell,i}u^{(i)})^2\right)\right] \leq L_\ell \mathrm{BE}_{\mathrm{mean}}^{\ell},\ \ell\in\mathcal{L}_2, \tag{3.19}$$

$$u^{(1)} \geq 0, \tag{3.20}$$

$$u^{(2)} \geq 0, \tag{3.21}$$

$$t \geq 0. \tag{3.22}$$

We further rewrite this problem equivalently as

$$\max_{u^{(1)},u^{(2)}} \quad t_1 + t_2 \tag{3.23}$$

$$N_i\alpha_i^\tau \bar{A}^{(i)}u^{(i)} + N_i\beta_i^\tau \left(\bar{A}^{(i)}u^{(i)}\right)^2 \geq t_i,\ i = 1, 2, \tag{3.24}$$

$$\sum_{i=1}^{2} \left(N_i\alpha_i^{\phi_\ell}(A_j^{\ell,i}u^{(i)}) + N_i\beta_i^{\phi_\ell}(A_j^{\ell,i}u^{(i)})^2\right) \leq \mathrm{BE}^\ell_{\max},\ j = 1, \ldots, L_\ell,\ \ell \in \mathcal{L}_1, \tag{3.25}$$

$$\sum_{i=1}^{2} \left[N_i\alpha_i^{\phi_\ell} \left(\sum_{j=1}^{L_\ell}(A_j^{\ell,i}u^{(i)})\right) + N_i\beta_i^{\phi_\ell} \left(\sum_{j=1}^{L_\ell}(A_j^{\ell,i}u^{(i)})^2\right)\right] \leq L_\ell \mathrm{BE}^\ell_{\mathrm{mean}},\ \ell \in \mathcal{L}_2, \tag{3.26}$$

$$u^{(1)} \geq 0, \tag{3.27}$$

$$u^{(2)} \geq 0, \tag{3.28}$$

$$t_1 \geq 0, \tag{3.29}$$

$$t_2 \geq 0. \tag{3.30}$$

The first advantage of this reformulation is that constraints (3.24) can be linearized. In particular, given that matrices $\bar{A}^{(i)}$ are nonnegative and the $u^{(i)} \geq 0$, constraints (3.24) hold if and only if constraints

$$\bar{A}^{(i)}u^{(i)} \geq \frac{-N_i\alpha_i^\tau + \sqrt{(N_i\alpha_i^\tau)^2 + 4N_i\beta_i^\tau t_i}}{2N_i\beta_i^\tau},\ i = 1, 2 \tag{3.31}$$

hold. In other words, the above problem can be equivalently reformulated as

$$P(t_1,t_2)\ \max_{u^{(1)},u^{(2)}}\ t_1+t_2 \tag{3.32}$$

$$\bar{A}^{(i)}u^{(i)} \geq \frac{-N_i\alpha_i^\tau+\sqrt{(N_i\alpha_i^\tau)^2+4N_i\beta_i^\tau t_i}}{2N_i\beta_i^\tau},\ i=1,2, \tag{3.33}$$

$$\sum_{i=1}^{2}\left(N_i\alpha_i^{\phi_\ell}(A_j^{\ell,i}u^{(i)})+N_i\beta_i^{\phi_\ell}(A_j^{\ell,i}u^{(i)})^2\right)\leq \mathrm{BE}^\ell_{\max},\ j=1,\ldots,L_\ell,\ \ell\in\mathcal{L}_1, \tag{3.34}$$

$$\sum_{i=1}^{2}\left[N_i\alpha_i^{\phi_\ell}\left(\sum_{j=1}^{L_\ell}(A_j^{\ell,i}u^{(i)})\right)+N_i\beta_i^{\phi_\ell}\left(\sum_{j=1}^{L_\ell}(A_j^{\ell,i}u^{(i)})^2\right)\right]\leq L_\ell\mathrm{BE}^\ell_{\mathrm{mean}},\ \ell\in\mathcal{L}_2, \tag{3.35}$$

$$u^{(1)}\geq 0, \tag{3.36}$$

$$u^{(2)}\geq 0, \tag{3.37}$$

$$t_1\geq 0, \tag{3.38}$$

$$t_2\geq 0. \tag{3.39}$$

Now the only thing that makes this problem nonconvex is the appearance of $\sqrt{t_i}$ on the RHS of constraints (3.33). We remedy this via a simple brute-force approximation approach. We discretize the $(t_1\geq 0, t_2\geq 0)$ quadrant with squares of size δ, and solve the above convex problem for every fixed (t_1,t_2) pair on the resulting grid. Furthermore, only a finite number of grid points need to be considered because it is easy to obtain a priori bounds on the largest possible values of t_1 and t_2. Specifically, the largest possible value of t_1 equals the optimal objective function value of problem (3.11)-(3.15) after setting $u^{(2)}=0$. Recall from the discussion above and from [69] that this is a single-modality and convex problem. Similarly, the largest possible value of t_2 equals the optimal objective function value of problem (3.11)-(3.15) after setting $u^{(1)}=0$. We denote these largest possible values by T_1^* and T_2^*, respectively. The resulting overall approximate solution procedure is summarized in Algorithm 1.

Note that as $\delta\to 0$, the approximate optimal value delivered by the above algorithm

Algorithm 1 Approximate solution of the spatiotemporally integrated modality selection problem

Require: Number of OAR voxels L_ℓ, for $\ell \in \mathcal{L}_2$; tolerance doses $\text{BE}^\ell_{\max}$ for $\ell \in \mathcal{L}_1$ and $\text{BE}^\ell_{\text{mean}}$ for $\ell \in \mathcal{L}_2$; dose-response parameters $\alpha_i^\tau, \beta_i^\tau$ for $i = 1, 2$; $\alpha_i^{\phi_\ell}, \beta_i^{\phi_\ell}$ for $\ell \in \mathcal{L}$ and $i = 1, 2$; dose-deposition matrices $\bar{A}^{(i)}$ for $i = 1, 2$; $A^{\ell,i}$, for $\ell \in \mathcal{L}$ and $i = 1, 2$; discretization parameter $\delta > 0$.

Solve the equivalent convex version of problem (3.11)-(3.15) after setting $u^{(2)} = 0$, linearizing constraint (3.12), and noting that the objective can be equivalently altered to $\bar{A}^{(1)}u^{(1)}$. Let T_1^* denote the optimal value of the original objective (3.11).

Solve the equivalent convex version of problem (3.11)-(3.15) after setting $u^{(1)} = 0$, linearizing constraint (3.12), and noting that the objective can be equivalently altered to $\bar{A}^{(2)}u^{(2)}$. Let T_2^* denote the optimal value of the original objective (3.11).

for $t_1 = 0 : \delta : T_1^*$ **do**
    for $t_2 = 0 : \delta : T_2^*$ **do**
        Solve $P(t_1, t_2)$; optimal value $= f^*(t_1, t_2)$; optimal solution $= u_*^{(1)}(t_1, t_2)$, $u_*^{(2)}(t_1, t_2)$
    end for
end for

$(t_1^*, t_2^*) = \underset{(t_1,t_2)}{\text{argmax}}\ f^*(t_1, t_2)$

Report $t_1^* + t_2^*$ as the approximate optimal value and $u_*^{(1)}(t_1^*, t_2^*)$, $u_*^{(2)}(t_1^*, t_2^*)$ as the approximate optimal solution of (P)

approaches the true optimal value of (P). One limitation of the above procedure is that depending on the value of δ, it calls for the solution of a large number of convex (feasibility) programs with linear and quadratic constraints, but with recent advances in convex optimization software, this is not a substantial hurdle.

Problem $P(t_1, t_2)$ can be rewritten in a standard linear-quadratic form using simple matrix algebra. This form facilitates implementation using off-the-shelf convex optimization software. To see this, let $'$ denote matrix and vector transpose. Observe that

$$N_i \beta_i^{\phi_\ell} \left(A_j^{\ell,i} u^{(i)} \right)^2 = \left(u^{(i)}\right)' \underbrace{\left(\sqrt{N_i \beta_i^{\phi_\ell}} A_j^{\ell,i} \right)' \left(\sqrt{N_i \beta_i^{\phi_\ell}} A_j^{\ell,i} \right)}_{Q_j^{\ell,i}} \left(u^{(i)}\right)$$

$$= \left(u^{(i)}\right)' Q_j^{\ell,i} \left(u^{(i)}\right), \ j = 1, \ldots, L_\ell, \ \ell \in \mathcal{L}, \ i = 1, 2.$$

Here, $Q_j^{\ell,i}$ is a square positive semi-definite matrix of size $K_1 \times K_1$ for $\ell \in \mathcal{L}_1$, and of size $K_2 \times K_2$ for $\ell \in \mathcal{L}_2$. In addition, for $\ell \in \mathcal{L}_1$ and $i = 1, 2$, define

$$G_j^{\ell,i} = N_i \alpha_i^{\phi_\ell} A_j^{\ell,i}, \ j = 1, \ldots, L_\ell.$$

Similarly, for $\ell \in \mathcal{L}_2$ and $i = 1, 2$, define

$$R^{\ell,i} = N_i \alpha_i^{\phi_\ell} \left(\sum_{j=1}^{L_\ell} A_j^{\ell,i} \right),$$

and

$$Q^{\ell,i} = \sum_{j=1}^{L_\ell} Q_j^{\ell,i}.$$

Now, define a collated column vector $u \in \Re^{K_1+K_2}$ of fluence-maps

$$u = \left[\begin{array}{c} u^{(1)} \\ u^{(2)} \end{array} \right].$$

For any integers $a \geq 1$ and $b \geq 1$, we use $0_{a,b}$ to denote an $a \times b$ matrix of zeros. Define

$$\tilde{G}_j^\ell = \left[\begin{array}{c|c} G_j^{\ell,1} & 0_{1,K_2} \end{array} \right] + \left[\begin{array}{c|c} 0_{1,K_1} & G_j^{\ell,2} \end{array} \right], \ \ell \in \mathcal{L}_1, \ j = 1, \ldots, L_\ell.$$

This is a row vector of length $K_1 + K_2$. Similarly, define a square positive semi-definite matrix of size $(K_1 + K_2) \times (K_1 + K_2)$ as

$$\tilde{Q}_j^\ell = \left[\begin{array}{c|c} Q_j^{\ell,1} & 0_{K_1,K_2} \\ \hline 0_{K_2,K_1} & Q_j^{\ell,2} \end{array}\right], \ \ell \in \mathcal{L}_1, \ j = 1, \ldots, L_\ell.$$

In addition, for $\ell \in \mathcal{L}_2$, define a row vector of length $K_1 + K_2$ as

$$\tilde{R}^\ell = \left[\begin{array}{c|c} R^{\ell,1} & 0_{1,K_2} \end{array}\right] + \left[\begin{array}{c|c} 0_{1,K_1} & R^{\ell,2} \end{array}\right],$$

and a square positive semi-definite matrix of size $(K_1 + K_2) \times (K_1 + K_2)$ as

$$\tilde{Q}^\ell = \left[\begin{array}{c|c} Q^{\ell,1} & 0_{K_1,K_2} \\ \hline 0_{K_2,K_1} & Q^{\ell,2} \end{array}\right].$$

Finally, define a matrix of size $2 \times (K_1 + K_2)$ as

$$\bar{A} = \left[\begin{array}{c|c} \bar{A}^{(1)} & 0_{1,K_2} \\ \hline 0_{1,K_1} & \bar{A}^{(2)} \end{array}\right],$$

and a column vector of length 2 as

$$c(t_1, t_2) = \left[\begin{array}{c} \frac{-N_1\alpha_1^\tau + \sqrt{(N_1\alpha_1^\tau)^2 + 4N_1\beta_1^\tau t_1}}{2N_1\beta_1^\tau} \\ \hline \frac{-N_2\alpha_2^\tau + \sqrt{(N_2\alpha_2^\tau)^2 + 4N_2\beta_2^\tau t_2}}{2N_2\beta_2^\tau} \end{array}\right].$$

Recall that Algorithm 1 only solves $P(t_1, t_2)$ for fixed values of pairs (t_1, t_2). That is, t_1, t_2 are not really variables. Thus, $P(t_1, t_2)$ reduces to a feasibility problem rather than an optimization problem. Then, $P(t_1, t_2)$ can be rewritten as

$$\max_u \ t_1 + t_2 \tag{3.40}$$

$$\bar{A}u \geq c(t_1, t_2), \tag{3.41}$$

$$\tilde{G}_j^\ell u + u'\tilde{Q}_j^\ell u \leq \mathrm{BE}_{\max}^\ell, \ j = 1, \ldots, L_\ell, \ \ell \in \mathcal{L}_1, \tag{3.42}$$

$$\tilde{R}^\ell u + u'\tilde{Q}^\ell u \leq L_\ell \mathrm{BE}_{\mathrm{mean}}^\ell, \ \ell \in \mathcal{L}_2, \tag{3.43}$$

$$u \geq 0. \tag{3.44}$$

3.3 Numerical results

We implemented the above solution procedure on a two-modality variation of the head-and-neck test case from [42, 43]. A schematic of the anatomy for this is shown in Figure 3.1. Here, modalities 1 and 2 correspond to photons and protons, respectively. Dose deposition matrices for photons were calculated using the tissue-phantom-ratio (TPR) lookup table method [41]. For protons, they were calculated using the approach in [55]. Computer code for this section was written in MATLAB running CVX toolbox for convex optimization [29].

The total number of treatment sessions, N, is fixed at 25, which is the conventional number as in Chapter 1. The parameter values are the same as in Chapter 1. Grid discretization, δ, is set to 5. Sensitivity analysis is conducted on biological characteristics of modality 2, by varying values of r as in Chapter 1. The value $r = 1$ is viewed as the base case as before. The biological effect on tumor of our best found solution (that is, the approximate optimal objective value) for different (N_1, N_2) pairs such that $N_1 + N_2 = 25$ and different values of r are reported in Table 3.3. Figure 3.2 plots the values from this table.

The table and figure display the following qualitative trends. For each fixed (N_1, N_2) pair, the biological effect on tumor is non-increasing as r increases. This holds because modality 2 inflicts higher damage to the OAR with increasing values of r. This, in effect, shrinks the feasible region and hence reduces the (approximate) optimal objective value. For $r = 0.8$, the largest biological effect on tumor (76.46) is attained for relatively larger values of N_2 as compared to that for $r = 1$ and $r = 1.2$. Again, this is because modality 2 is more desirable for smaller values of r and hence it is better to use a larger number of treatment sessions with modality 2. In fact, for $r = 1.2$, the best tumor biological effect is attained by using $N_1 = 25$ and $N_2 = 0$, which corresponds to not using modality 2 at all. For smaller values of r, administering a combination of two modalities (that is, $0 < N_1, N_2 < 25$) produces a higher tumor biological effect than using any single modality ($N_1 = 25$ or $N_2 = 25$).

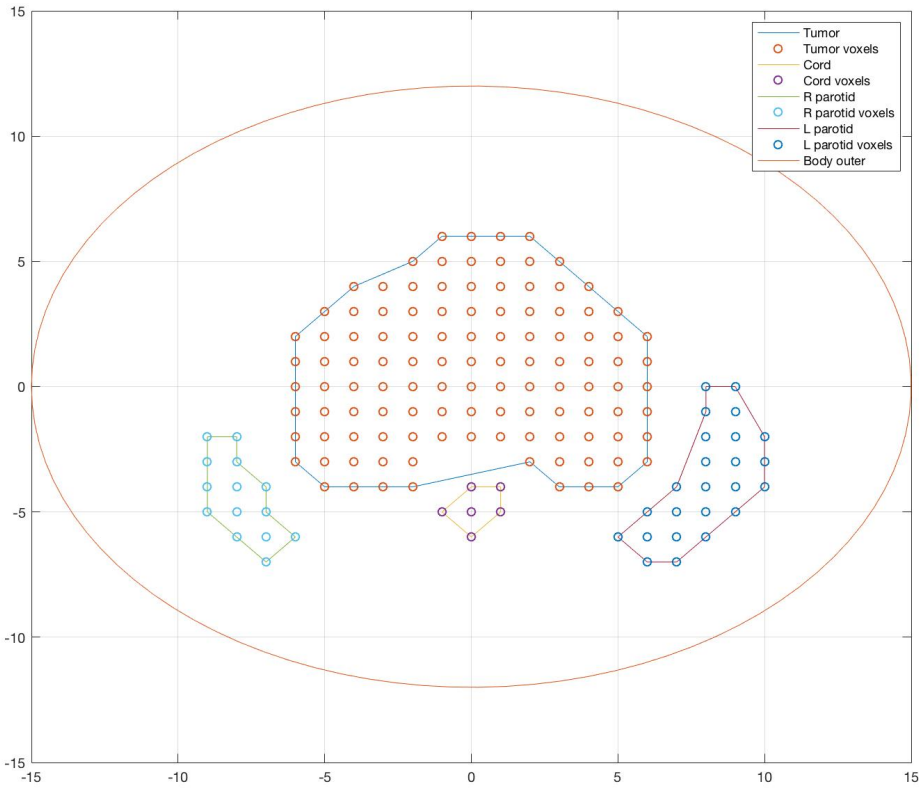

Figure 3.1: The head-and-neck geometry used for numerical experiments.

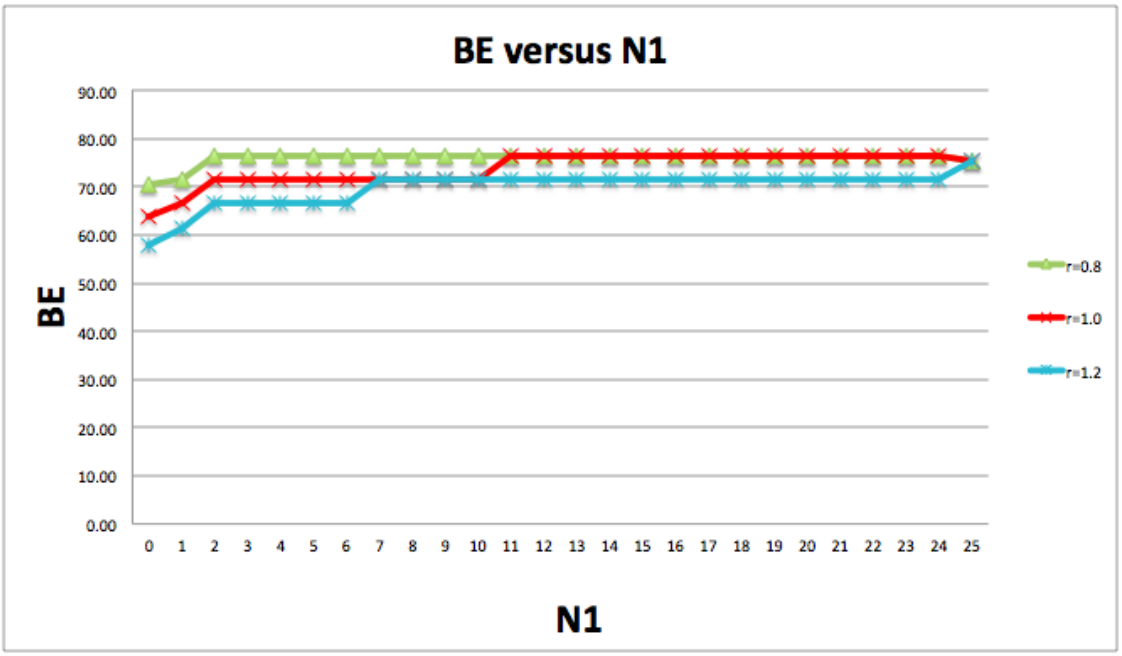

Figure 3.2: Biological effect of the best found modality (or combination) for every N_1 value, where total N is fixed at 25.

N1	N2	r=0.8	r=1.0	r=1.2
0	25	70.29	63.70	57.87
1	24	71.46	66.46	61.46
2	23	76.46	71.46	66.46
3	22	76.46	71.46	66.46
4	21	76.46	71.46	66.46
5	20	76.46	71.46	66.46
6	19	76.46	71.46	66.46
7	18	76.46	71.46	71.46
8	17	76.46	71.46	71.46
9	16	76.46	71.46	71.46
10	15	76.46	71.46	71.46
11	14	76.46	76.46	71.46
12	13	76.46	76.46	71.46
13	12	76.46	76.46	71.46
14	11	76.46	76.46	71.46
15	10	76.46	76.46	71.46
16	9	76.46	76.46	71.46
17	8	76.46	76.46	71.46
18	7	76.46	76.46	71.46
19	6	76.46	76.46	71.46
20	5	76.46	76.46	71.46
21	4	76.46	76.46	71.46
22	3	76.46	76.46	71.46
23	2	76.46	76.46	71.46
24	1	76.46	76.46	71.46
25	0	75.27	75.27	75.27

Table 3.1: Biological effect of best found solution on tumor for different values of r and (N_1, N_2) pairs.

3.4 Conclusions

We studied the spatiotemporally integrated extension of the model in Chapter 1 by directly optimizing radiation intensity profiles for the two modalities. The model is a non-convex QCQP. We developed an approximate solution method rooted in convex optimization. Numerical sensitivity analysis was performed to gain insights into how biological properties of modality 2 affect the choice of modality and the biological effect on tumor. These insights and qualitative trends in our results matched with clinical intuition, which validates our problem formulation and solution method. This validation is important because this chapter is the first-ever attempt at modeling a spatiotemporally integrated version of the modality selection problem. It may be interesting in the future to investigate whether or not the formulation and solution method in this chapter can be extended to a robust counterpart.

BIBLIOGRAPHY

[1] A Ahamad, D I Rosenthal, and K K Ang. *Squamous cell head and neck cancer : recent clinical progress and prospects for the future*. Current Clinical Oncology. Humana Press, Totowa, New Jersey, USA, 2005.

[2] P H Ahn, J N Lukens, B-K K Teo, M Kirk, and A Lin. The use of proton therapy in the treatment of head and neck cancers. *The Cancer Journal*, 20(6):421–426, 2014.

[3] A Ajdari and A Ghate. Robust spatiotemporally integrated fractionation in radiotherapy. *Operations Research Letters*, 44(4):544–549, 2016.

[4] G Arcangeli, B Saracino, S Gomellini, M G Petrongari, S Arcangeli, S Sentinelli, S Marzi, V Landoni, J Fowler, and L Strigari. A prospective phase iii randomized trial of hypofractionation versus conventional fractionation in patients with high-risk prostate cancer. *International Journal of Radiation Oncology Biology Physics*, 78(1):11–18, 2010.

[5] C I Armpilia, R G Dale, and B Jones. Determination of the optimum dose per fraction in fractionated radiotherapy when there is delayed onset of tumour repopulation during treatment. *The British Journal of Radiology*, 77(921):765–767, 2004.

[6] H Badri, Y Watanabe, and K Leder. Optimal radiotherapy dose schedules under parametric uncertainty. *Physics in Medicine and Biology*, 61(1):338, 2016.

[7] M Baumann, M Krause, J Overgaard, J Debus, S M Bentzen, J Daartz, C Richter, D Zips, and T Bortfeld. Radiation oncology in the era of precision medicine. *Nature Reviews Cancer*, 16:234–249, 2016.

[8] D Bertsimas, D B Brown, and C Caramanis. Theory and applications of robust optimization. *SIAM Review*, 53(3):464–501, 2011.

[9] A Bertuzzi, C Bruni F Papa, and C Sinisgalli. Optimal solution for a cancer radiotherapy problem. *Journal of Mathematical Biology*, 66(1-2):311–349, 2013.

[10] R B Bonnet, D Bush, G A Cheek, J D Slater, D Panossian, C Franke, and J M Slater. Effects of proton and combined proton/photon beam radiation on pulmonary function in patients with resectable but medically inoperable non-small cell lung cancer. *Chest*, 120(6):1803–1810, 2001.

[11] T Bortfeld, J Ramakrishnan, J N Tsitsiklis, and J Unkelbach. Optimization of radiotherapy fractionation schedules in the presence of tumor repopluation. *INFORMS Journal on Computing*, 27(4):788–803, 2015.

[12] S Boyd and L Vandenberghe. *Convex Optimization*. Cambridge University Press, Cambridge, UK, 2004.

[13] Z Chen, J Wang, and W Hu. SU-F-T-199: A new strategy for integrating photon with proton and carbon ion in the treatment planning. *Medical Physics*, 43(6Part15):3507–3508, 2016.

[14] A L A J Dekker, S L Gulliford, M A Ebert, and C G Orton. Point/counterpoint: Future radiotherapy practice will be based on evidence from retrospective interrogation of linked clinical data sources rather than prospective randomized controlled clinical trials. *Medical Physics*, 41(3):1–3, 2014.

[15] T F DeLaney, , N J Liebsch, F X Pedlow, J Adams, E A Weyman, B Y Yeap, N Depauw, G P Nielsen, D C Harmon, S S Yoon, Y L Chen, J H Schwab, and F J Hornicek. Long-term results of phase ii study of high dose photon/proton radiotherapy in the management of spine chordomas, chondrosarcomas, and other sarcomas. *Journal of Surgical Oncology*, 110(2):115–122, 2014.

[16] T F DeLaney. Phase II study of high-dose photon/proton radiotherapy in the manage-

ment of spine sarcomas. *International Journal of Radiation Oncology Biology Physics*, 74(3):732–739, 2009.

[17] T F DeLaney. Proton therapy in the clinic. *Frontiers of Radiation Therapy and Oncology*, 43:465–485, 2011.

[18] D K Ebner and T Kamada. The emerging role of carbon-ion radiotherapy. *Frontiers in Oncology*, 6(140):1–6, 2016.

[19] L Feuvret, G Noel, D C Weber, P Pommier, R Ferrand, L De Marzi, F Dhermain, and C Alapetite. A treatment planning comparison of combined photon–proton beams versus proton beams–only for the treatment of skull base tumors. *International Journal of Radiation Oncology Biology Physics*, 69(3):944–954, 2007.

[20] J F Fowler. How worthwhile are short schedules in radiotherapy?: A series of exploratory calculations. *Radiotherapy and Oncology*, 18(2):165–181, 1990.

[21] J F Fowler. Biological factors influencing optimum fractionation in radiation therapy. *Acta Oncologica*, 40(6):712–717, 2001.

[22] J F Fowler. Is there an optimal overall time for head and neck radiotherapy? a review with new modeling. *Clinical Oncology*, 19(1):8–27, 2007.

[23] J F Fowler. Optimum overall times ii: Extended modelling for head and neck radiotherapy. *Clinical Oncology*, 20(2):113–126, 2008.

[24] J F Fowler. Sensitivity analysis of parameters in linear-quadratic radiobiologic modeling. *International Journal of Radiation Oncology Biology Physics*, 73(5):1532–1537, 2009.

[25] J F Fowler and M A Ritter. A rationale for fractionation for slowly proliferating tumors such as prostatic adenocarcinoma. *International Journal of Radiation Oncology Biology Physics*, 32(2):521–529, 1995.

[26] K K Fu, T F Pajak, A Trotti, C U Jones, S A Spencer, T L Phillips, A S Garden, J A Ridge, J S Cooper, and K K Ang. A radiation therapy oncology group (RTOG) phase iii randomized study to compare hyperfractionation and two variants of accelerated fractionation to standard fractionation radiotherapy for head and neck squamous cell carcinomas: first report of RTOG 9003. *International Journal of Radiation Oncology Biology Physics*, 48(1):7 – 16, 2000.

[27] A S Garden. Altered fractionation for head and neck cancer. *Oncology*, 15(10):1326–1332, 2001.

[28] M Goitein and J D Cox. Should randomized clinical trials be required for proton radiotherapy. *Journal of Clinical Oncology*, 26(2):175–176, 2008.

[29] M Grant and S Boyd. CVX: MATLAB software for disciplined convex programming (web page and software), 2009.

[30] J P Grutters, A G H Kessels, M Pijls-Johannesma, D De Ruysscher, M A Joore, and P Lambin. Comparison of the effectiveness of radiotherapy with photons, protons and carbon-ions for non-small cell lung cancer: A meta-analysis. *Radiotherapy and Oncology*, 95(1):32–40, 2010.

[31] E J Hall and A J Giaccia. *Radiobiology for the Radiologist*. Lippincott Williams & Wilkins, Philadelphia, Pennsylvania, USA, 2005.

[32] E C Halperin. Particle therapy and treatment of cancer. *Lancet Oncology*, 7(8):676–685, 2006.

[33] E C Halperin, L W Brady, and C A Perez. *Perez and Brady's Principles and Practice of Radiation Oncology*. Lippincott Williams and Wilkins (Wolters Kluwer Health), Philadelphia, PA, USA, 2013.

[34] K A Higgins, K O'Connell, Y Liu, T W Gillespie, M W Mcdonald, R N Pillai, K R Patel, P R Patel, C G Robinson, C B Simone, T K Owonikoko, C P Belani, F R Khuri, W J

Curran, S S Ramalingam, and M Behera. National cancer database analysis of proton versus photon radiation therapy in non-small cell lung cancer. *International Journal of Radiation Oncology Biology Physics*, 97(1):128–137, 2017.

[35] K F Ho, J F Fowler, A J Sykes, B K Yap, L W Lee, and N J Slevin. Imrt dose fractionation for head and neck cancer: Variation in current approaches will make standardisation difficult. *Acta Oncologica*, 3(431-439):2009, 48.

[36] J C Horiot, P Bontemps, W van den Bogaert, R L Fur, D van den Weijngaert, M Bolla, J Bernier, A Lusinchi, M Stuschke, J Lopez-Torrecilla, A C Begg, M Pierart, and L Collette. Accelerated fractionation (AF) compared to conventional fractionation (CF) improves loco-regional control in the radiotherapy of advanced head and neck cancers: Results of the eortc 22851 randomized trial. *Radiotherapy and Oncology : Journal of the European Society for Therapeutic Radiology and Oncology*, 44(2):111–121, 1997.

[37] J C Horiot, R Le Fur, T N'Guyen, C Chenal, S Schraub, S Alfonsi, G Gardani, W Van Den Bogaert, S Danczak, and M Bolla. Hyperfractionation versus conventional fractionation in oropharyngeal carcinoma: final analysis of a randomized trial of the eortc cooperative group of radiotherapy. *Radiotherapy Oncology*, 25(4):231–241, December 1992.

[38] B Jones, L T Tan, and R G Dale. Derivation of the optimum dose per fraction from the linear quadratic model. *The British Journal of Radiology*, 68(812):894–902, 1995.

[39] H A Kader, A R Mydin, M Wilson, C Alexander, J Shahi, I Pathak, J S Wu, and P T Truong. Treatment outcomes of locally advanced oropharyngeal cancer: A comparison between combined modality radio-chemotherapy and two variants of single modality altered fractionation radiotherapy. *International Journal of Radiation Oncology Biology Physics*, 80(4):1030 – 1036, 2011.

[40] H Keller, G Meier, A Hope, and M Davison. Fractionation schedule optimization for lung

cancer treatments using radiobiological and dose distribution characteristics. *Medical Physics*, 39(6):3811–3811, 2012.

[41] F M Khan. *The Physica of Radiation Therapy*. Lippincott Williams & Wilkins, Baltimore, Maryland, USA, fourth edition, 2010.

[42] M Kim. *A Mathematical Framework for Spatiotemporal Optimality in Radiation Therapy*. PhD thesis, University of Washington, Seattle, Washington, USA, 2010.

[43] Minsun Kim, Archis Ghate, and Mark H. Phillips. A stochastic control formalism for dynamic biologically conformal radiation therapy. *European Journal of Operational Research*, 219(3):541 – 556, 2012.

[44] P Lambin, J Zindler, B G L Vanneste, L V De Voorde, D Eekers, I Compter, K M Panth, J Peerlings, R T H M Larue, T M Deist, A Jochems, T Lustberg, J van Soest, E E C de Jong, A J G Even, B Reymen, N Rekers, M van Gisbergen, E Roelofs, S Carvalho, R T H Leijenaar, C M L Zegers, M Jacobs, J van Timmeren, P Brouwers, J A Lal, L Dubois, A Yaromina, E J Van Limbergen, M Berbee, W van Elmpt, C Oberije, B Ramaekers, A L A J Dekker, L J Boersma, F Hoebers, K M Smits, A J Berlanga, and S Walsh. Decision support systems for personalized and participative radiation oncology. *Advanced Drug Delivery Reviews*, 109:131–153, 2017.

[45] T S Lawrence, R K Ten Hakken, and A Giaccia. *Principles of Radiation Oncology*. Lippincott Williams and Wilkins, Philadelphia, PA, USA, 2008.

[46] J S Loeffler and M Durante. Charged particle therapy-optimization, challenges and future directions. *Nature Reviews Clinical Oncology*, 10(7):411–424, 2013.

[47] Z-Q Luo, W-K Ma, A M C So, and Y Ye. Semidefinite relaxation of quadratic optimization problems. *IEEE Signal Processing Magazine*, 27(3):20–34, 2010.

[48] S Di Maio, S Yip, G A Al Zhrani, F E Alotaibi, A Al Turki, E Kong, and R C Rostomily. Novel targeted therapies in chordoma: an update. *Therapeutics and Clinical Risk Management*, 11:873–883, 2015.

[49] L B Marks, E D Yorke, A Jackson, R K Ten Haken, L S Constine, A Eisbruch, S M Bentzen, J Nam, and J O Deasy. Use of normal tissue complication probability models in the clinic. *International Journal of Radiation Oncology Biology Physics*, 76(3):S10–S19, 2010.

[50] S Marzi, B Saracino, M Petrongari, S Arcangeli, S Gomellini, G Arcangeli, M Benassi, and V Landoni. Modeling of alpha/beta for late rectal toxicity from a randomized phase ii study: conventional versus hypofractionated scheme for localized prostate cancer. *Journal of Experimental & Clinical Cancer Research*, 28(1):117–124, 2009.

[51] P N McDermott. *Tutorials in Radiotherapy Physics: Advanced Topics with Problems and Solutions*. CRC Press, 2016.

[52] T Mitin and A L Zietman. Promise and pitfalls of heavy-particle therapy. *Journal of Clinical Oncology*, 32(26):2855–2863, 2014.

[53] M Mizuta, S Takao, H Date, N Kishimoto, K L Sutherland, R Onimaru, and H Shirato. A mathematical study to select fractionation regimen based on physical dose distribution and the linear-quadratic model. *International Journal of Radiation Oncology Biology Physics*, 84(3):829 – 833, 2012.

[54] J P Morgan. A patient's perspective on randomized clinical trials for proton radiotherapy. *Journal of Clinical Oncology*, 26(15):2592, 2008.

[55] S Nill, U Oelfke, and T Bortfeld. A new planning tool for IMRT treatments: implmentation and first application for proton beams. In W Schlegel and T Bortfeld, editors, *The use of computers in radiation therapy*, pages 326–328, Berlin, Germany, 2000. Springer.

[56] H Paganetti. Range uncertainties in proton therapy and the role of Monte Carlo simulations. *Physics in Medicine and Biology*, 57(11):R99–R117, 2012.

[57] H Paganetti. Relative biological effectiveness (RBE) values for proton beam therapy. Variations as a function of biological endpoint, dose, and linear energy transfer. *Physics in Medicine and Biology*, 59(2):R419–R472, 2014.

[58] H Paganetti, A Niemierko, M Ancukiewicz, L E Gerweck, M Goitein, J S Loeffler, and H D Suit. Relative biological effectiveness (RBE) values for proton beam therapy. *International Journal of Radiation Oncology Biology Physics*, 53(2):407–421, 2002.

[59] H Paganetti and P van Luijk. Biological considerations when comparing proton therapy with photon therapy. *Seminars in Radiation Oncology*, 23(2):77–87, 2013.

[60] J Park and S Boyd. General heuristics for nonconvex quadratically constrained quadratic programming. `https://arxiv.org/abs/1703.07870`, May 2017.

[61] A Peeters, J Grutters, M Pijls-Johannesma, S Reimoser, D De Ruysscher, J L Severens, M A Joore, and P Lambin. How costly is particle therapy? cost analysis of external beam radiotherapy with carbon-ions, protons and photons. *Radiation Research*, 95(1):45–53, 2010.

[62] X S Qi, Q Yang, S P Lee, X A Li, and D Wang. An estimation of radiobiological parameters for head-and-neck cancer cells and the clinical implications. *Cancers*, 4:566–580, 2012.

[63] B L Ramaekers, J P Grutters, M Pijls-Johannesma, P Lambin, M A Joore, and J A Langendijk. Protons in head-and-neck cancer: Bridging the gap of evidence. *International Journal of Radiation Oncology Biology Physics*, 85(5):1282–1288, 2013.

[64] B L Ramaekers, M Pijls-Johannesma, M A Joore, P van den Ende, J A Langendijk, P Lambin, A G H Kessels, and J P Grutters. Systematic review and meta-analysis of

radiotherapy in various head and neck cancers: Comparing photons, carbon-ions and protons. *Cancer Treatment Reviews*, 37(3):185–201, 2011.

[65] S Rockwell. Experimental radiotherapy: a brief history. *Radiation Research*, 150(Supplement):S157–S169, November 1998.

[66] Y Rong and J Welsh. Basics of particle therapy II biologic and dosimetric aspects of clinical hadron therapy. *American Journal of Clinical Oncology*, 33(6):646–649, 2010.

[67] F Saberian, A Ghate, and M Kim. A two-variable linear program solves the standard linear-quadratic formulation of the fractionation problem in cancer radiotherapy. *Operations Research Letters*, 43(3):254–258, 2015.

[68] F Saberian, A Ghate, and M Kim. Optimal fractionation in radiotherapy with multiple normal tissues. *Mathematical Medicine and Biology*, 33(2):211–252, 2016.

[69] F Saberian, A Ghate, and M Kim. Spatiotemporally optimal fractionation in radiotherapy. *INFORMS Journal on Computing*, 29(3):422–437, 2017.

[70] D Schaue and W H Mcbride. Opportunities and challenges of radiotherapy for treating cancer. *Nature Reviews Clinical Oncology*, 12(9):527–540, 2015.

[71] K C Schiller, G Habl, and S E Combs. Protons, photons, and the prostate –is there emerging evidence in the ongoing discussion on particle therapy for the treatment of prostate cancer? *Frontiers in Oncology*, 6:8, 2016.

[72] R J Schulz and A R Kagan. Carbon-ion therapy: One more step in the endless quest for the ideal dose distribution. *International Journal of Radiation Oncology Biology Physics*, 95(1):561, 2016.

[73] D Schulz-Ertner, O Jakel, and W Schlegel. Radiation therapy with charged particles. *Seminars in Radiation Oncology*, 16(4):249–259, 2006.

[74] D Schulz-Ertner and H Tsujii. Particle radiation therapy using proton and heavier ion beams. *Journal of Clinical Oncology*, 25(8):953–964, 2007.

[75] H D Thames, S M Bentzen, I Turesson, M Overgaard, and W van den Bogaert. Fractionation parameters for human tissues and tumors. *International Journal Radiation Biology*, 56(5):701–710, 1989.

[76] F Tommsino, E Scifoni, and M Durante. New ions for therapy. *International Journal of Particle Therapy*, 2(3):428–438, 2015.

[77] M A Torres, E L Chang, A Mahajan, D G Lege, B A Riley, X Zhang, M Lii, D G Kornguth, C E Pelloski, and S Y Woo. Optimal treatment planning for skull base chordoma: photons, protons, or a combination of both? *International Journal of Radiation Oncology Biology Physics*, 74(4):1033–1039, 2009.

[78] A Trotti, K K Fu, T F Pajak, C U Jones, S A Spencer, T L Phillips, A S Garden, J A Ridge, J S Cooper, and K K Ang. Long term outcomes of RTOG 90–03: A comparison of hyperfractionation and two variants of accelerated fractionation to standard fractionation radiotherapy for head and neck squamous cell carcinoma. *International Journal of Radiation Oncology Biology Physics*, 63(Supplement 1):S70–S71, 2005.

[79] M D Tyson, D F Penson, and M J Resnick. The comparative oncologic effectiveness of available management strategies for clinically localized prostate cancer. *Urologic Oncology: Seminars and Original Investigations*, 35(2):51–58, 2017.

[80] J Unkelbach, D Craft, E Saleri, J Ramakrishnan, and T Bortfeld. The dependence of optimal fractionation schemes on the spatial dose distribution. *Physics in Medicine and Biology*, 58(1):159–167, 2013.

[81] J Unkelbach, C Zeng, and M Engelsman. Simultaneous optimization of dose distributions and fractionation schemes in particle radiotherapy. *Medical Physics*, 40(9):091702, 2013.

[82] J van Loon, J P Grutters, and F Macbeth. Evaluation of novel radiotherapy technologies: what evidence is needed to assess their clinical and cost effectiveness, and how should we get it? *Lancet Oncology*, 13(4):e169–e177, 2012.

[83] M V Williams, J Denekamp, and J F Fowler. A review of alpha/beta ratios for experimental tumors: implications for clinical studies of altered fractionation. *International Journal of Radiation Oncology Biology Physics*, 11(1):87–96, January 1985.

[84] H Rodney Withers. Biologic basis for altered fractionation schemes. *Cancer*, 55(S9):2086–2095, 1985.

[85] Y Yang and L Xing. Optimization of radiotherapy dose-time fractionation with consideration of tumor specific biology. *Medical Physics*, 32(12):3666–3677, 2005.

[86] L T Yonemoto, J D Slater, C J Rossi Jr, J E Antoine, L Loredo, J O Archambeau, R W Schulte, D W Miller, S L Teichman, and J M Slater. Combined proton and photon conformal radiation therapy for locally advanced carcinoma of the prostate: Preliminary results of a phase I/II study. *International Journal of Radiation Oncology Biology Physics*, 37(1):21–29, 1997.

ACKNOWLEDGEMENTS

I am grateful to my advisors Dr. Archis Ghate and Dr. Minsun Kim for their supervisions and funding through these years. I also would like to thank Dr. Zelda Zabinsky and Dr. Michael Wagner for serving on my committee. I am thankful to the

To my parents who sacrificed a lot for me, many thanks for your unconditional love, patience, and selfless support through my studies and life in general. Specially, I would like to show my deepest gratitude to my mother for her continuous encouragements and emotional support through these years. This would not be possible without you.

To my family members Siamak, Abazar, Farzad, Farnaz and Elnaz, thank you for your continuous love and support. I feel so lucky to have you in my life. Also to my boyfriend, Shayan who was so encouraging, thank you for your love and support.

I would like to thank my uncle Qumars who although no longer with us, continues to be inspiring for me. I also would like to thank my aunt Shahla for her love and support through these years.

Last but not least, to my little nephews, Sami and Mani who cheered me up with their cute lovely words, pictures and videos even during my hardest time, thank you so much for your love and support. I feel so lucky to be your aunt.